

# We are IntechOpen, the world's leading publisher of Open Access books Built by scientists, for scientists

7,000

Open access books available

186,000

International authors and editors

200M

Downloads

Our authors are among the

154

Countries delivered to

TOP 1%

most cited scientists

12.2%

Contributors from top 500 universities



WEB OF SCIENCE™

Selection of our books indexed in the Book Citation Index  
in Web of Science™ Core Collection (BKCI)

Interested in publishing with us?  
Contact [book.department@intechopen.com](mailto:book.department@intechopen.com)

Numbers displayed above are based on latest data collected.  
For more information visit [www.intechopen.com](http://www.intechopen.com)



Chapter

# Upconversion Luminescent Nanoparticles and Their Biomedical Applications in Imaging

*Dalia Chávez-García and Mario Guzman*

## Abstract

Nanomaterials offer promising solutions for chemotherapy challenges, addressing issues like cytotoxicity and biocompatibility. In cancer clinical protocols, biomedical imaging is vital, providing insights into tumor morphology. Luminescent nanomaterials or nanoparticles (LNPs), particularly effective for diseases like cancer, possess controllable properties like size (usually  $<100$  nm), surface charge, and external functionalization. LNPs interact with biological systems at systemic and cellular levels. Cellular uptake is crucial, allowing selective targeting of cancer cells through overexpressed surface receptors such as transferrin receptor (TfR), G-protein coupled receptor (GPCR), folate receptor (FR), epidermal growth factor receptor (EGFR), lectins, and low-density lipoprotein receptor (LDLR). LNPs can accumulate in subcellular compartments, playing a pivotal role in drug delivery. Studies explore LNPs' internalization into cells, investigating their potential to deliver cargoes like DNA, siRNA, miRNA, and small-molecule drugs. This review highlights the latest advancements in LNPs and their biomedical applications. Despite these promising developments, comprehensive nanotoxicological assessments are crucial for a better understanding of LNPs' behavior in biological systems, paving the way for future clinical applications.

**Keywords:** rare earth, upconversion luminescent, near-infrared, biological imaging, nanotoxicological assessment

## 1. Introduction

Nanomaterials possess unique physical properties, including magnetic, optical, mechanical, and electrical properties, which are influenced by quantum mechanics, such as electron configuration and confinement. These properties are closely linked to the size of materials produced at the nanoscale [1]. Traditionally, one-photon imaging technique that detects light emission in the visible spectra (400–700 nm) has been commonly used for in vivo optical imaging. However, in the past decade, the near-infrared (NIR-I; 700–900 nm) spectra has gained prominence due to the high light scattering coefficient of live tissues and their autofluorescence. Moreover, there is a growing interest in optical imaging in the second

near-infrared (NIR-II; 1000–1700 nm) spectra, utilizing fluorescent or luminescent probes based on various materials, including inorganic quantum dots (QDs), polymer-encapsulated organic dyes, and nanoparticles [1, 2]. Researchers have developed luminescent upconversion nanoparticles (UCNPs) for NIR-I bioimaging of disease models in live mice, enhancing visualization of molecular and biological processes, as well as aiding molecular targeting-based therapies and diagnosis [3–5].

LNPs also known as phosphors or nanophosphors are solid materials capable of converting various forms of energy into electromagnetic radiation, typically in the visible range. However, they can also emit radiation in the infrared (IR), X-ray, or ultraviolet (UV) regions [6]. Particularly, UCNPs have the ability to convert NIR energy into visible light. Some types of UCNPs have a combination of Yb ions with other lanthanide ions. The  $\text{Yb}^{3+}$  ion possesses an energy-level scheme characterized by a single excited 4f level of  $^2f_{5/2}$  [2]. It exhibits an absorption band centered at 980 nm, attributed to the  $^2F_{7/2} \rightarrow ^2F_{5/2}$  transition. This absorption band resonates with multiple f-f transitions in upconverting lanthanide ions such as  $\text{Tm}^{3+}$ ,  $\text{Ho}^{3+}$ , and  $\text{Er}^{3+}$ . Consequently, the  $\text{Yb}^{3+}$  ion is widely employed as a sensitizer. Furthermore, the luminescence of  $\text{Yb}^{3+}$  falls within the range of 960–1040 nm, making it a potential candidate for activators in NIR-II probes.

This review aims to showcase different studies involving UCNPs in bioimaging for both in vivo and in vitro applications. In the subsequent section, we will delve into the various types of luminescent nanomaterials to enhance our understanding of the underlying quantum processes involved.

## 2. Luminescent nanomaterials

Different types of luminescence phenomena exist based on the source of the excitation thus:

- **Photoluminescence:** This occurs when the nanomaterial is excited by electromagnetic energy, such as ultraviolet or infrared radiation.
- **Cathodoluminescence:** Excitation takes place when the nanomaterial is exposed to a beam of high-energy electrons.
- **Triboluminescence:** Mechanical energy triggers luminescence in the nanomaterial.
- **Electroluminescence:** Application of an electric voltage excites the nanomaterial, leading to luminescence.
- **X-ray luminescence:** Luminescence is induced when the nanomaterial interacts with X-rays.
- **Chemiluminescence:** Luminescence arises from a chemical reaction.

The luminescence of a material involves several physical processes:

1. **Energy absorption:** An activator ion or another ion, known as a sensitizer, absorbs the energy and transfers it to the host lattice or the activator ion.

2. Energy emission: The activator ion releases the absorbed energy, resulting in visible spectrum emission.
3. Relaxation to the ground state: The material returns to its ground state through non-radiative processes.
4. Interaction between luminescent centers: Energy transfer occurs between different luminescent centers.

These processes collectively contribute to the luminescent properties exhibited by nanomaterials. The host lattice plays a significant role in the luminescent process as its optical properties can vary. The ion absorbing the energy can exhibit different spectral properties depending on the host lattice, primarily influenced by factors such as covalency. Higher covalency leads to a reduction in electron interactions, causing electronic transitions between energy levels to shift to lower energy levels. For instance, the  $\text{Eu}^{3+}$  ion commonly employed in LMN exhibits a higher energy absorption band when situated in the fluoride  $\text{YF}_3$  compared to the covalent oxide  $\text{Y}_2\text{O}_3$ . Consequently, greater energy is required to excite  $\text{Eu}^{3+}$  when it is in a fluoride compared to a covalent oxide [6, 7]. In this review, the focus will be on upconversion luminescent nanomaterials (UCNPs). Downconversion luminescent nanomaterials (DCNPs), on the other hand, require higher excitation energies, such as UV energy, and emit in the visible range. In contrast, UCNPs emit at higher energy wavelengths in the visible range and are excited by lower energy sources, such as near-infrared (NIR) radiation. Various types of upconversion processes exist [8]:

- Energy transfer, known as the APTE effect (Addition de Photons Par Transfers d'Énergie), where ions sequentially transfer their excitation energy to another ion that can emit from a higher energy level.
- Two-step absorption, which involves a single ion with dual absorption.
- Cooperative sensitization, where two ions simultaneously transfer their excitation energy to another ion, leading to emission from the excited level.
- Cooperative luminescence, where two ions combine their excitation energy to emit a single quantum.
- Second harmonic generation (frequency doubling), which doubles the frequency of the incident light without involving any absorption transitions.
- Two-photon absorption, where two photons are simultaneously absorbed without an intermediary energy level, and emission occurs from the excited energy level.

These different processes contribute to the unique upconversion luminescence observed in nanomaterials. **Tables 1–3** showcase various types of upconversion luminescent nanomaterials (UCNPs) utilizing different host lattices, with the trivalent Yb ion serving as a sensitizer.

Research on the development of UCNPs has been ongoing for over 20 years and continues to progress. Numerous researchers have dedicated their efforts to exploring

Host lattice	Sensitizer ion	Activator ion	Emission (s) (nm)	Reference
<b>Oxides</b>				
Y <sub>2</sub> O <sub>3</sub>	Yb	Er	660	[9, 10]
Y <sub>2</sub> O <sub>3</sub>	Yb	Ho	549,666	[11, 12]
Lu <sub>2</sub> O <sub>3</sub>	Yb	Er, Tm	662,477,490	[13, 14]
Y <sub>2</sub> O <sub>3</sub>	Yb	Er, Tm	550,660	[15, 16]
Gd <sub>2</sub> O <sub>3</sub>	Yb	Er	600, 660	[17, 18]
La <sub>2</sub> O <sub>3</sub>	Yb	Er	530,549,659,672	[19]
<b>Oxysulfides</b>				
Y <sub>2</sub> O <sub>2</sub> S	Yb	Er	520–560,650–700	[20, 21]
Y <sub>2</sub> O <sub>2</sub> S	Yb	Tm	450–500,650,690	[22, 23]
Gd <sub>2</sub> O <sub>2</sub> S	Yb	Er	520–580,650–700	[23, 24]
<b>Oxyhalides</b>				
GdOF	Yb	Er	521,545,656	[25, 26]
YOF	Yb	Er	525,545,656	[27, 28]

**Table 1.**  
UCNP detailed with NIR excitation. Oxides, oxysulfides, and oxyhalides.

Host lattice	Sensitizer ion	Activator ion	Emission (s) (nm)	Reference
<b>Phosphates</b>				
LaPO <sub>4</sub>	Yb	Er	535–556	[29, 30]
LuPO <sub>4</sub>	Yb	Tm	476	[31]
<b>Molybdates</b>				
La <sub>2</sub> (MoO <sub>4</sub> ) <sub>3</sub>	Yb	Er	519,541	[32, 33]
La <sub>2</sub> (MoO <sub>4</sub> ) <sub>3</sub>	Yb	Tm	472,647	[34]
<b>Tungstates</b>				
NaY(WO <sub>4</sub> ) <sub>2</sub>	Yb	Er	526,553,660	[35, 36]
NaY(WO <sub>4</sub> ) <sub>2</sub>	Yb	Tm	476,647	[12, 35, 36]
<b>Gallates</b>				
Gd <sub>3</sub> Ga <sub>5</sub> O <sub>12</sub>	Yb	Tm	454,484,640–680	[37, 38]
<b>Vanadate</b>				
YVO <sub>4</sub>	Yb	Er	N/A	[39, 40]

**Table 2.**  
UCNP detailed with NIR excitation. Phosphates, molybdates, tungstates, gallates, and vanadates.

and identifying UCNP with optimal luminescent properties in specific host lattices. **Tables 1–3** present a comprehensive overview of the various types of UCNP created using different host lattices and dopant ions.

The intensity of luminescence in different combinations of ions is influenced by both the host lattice and ion doping. It is important to note that high doping

Host lattice	Sensitizer ion	Activator ion	Emission (s) (nanometers)	Reference
Fluorides				
LaF <sub>3</sub>	Yb	Er	521,545,659	[41, 42]
LaF <sub>3</sub>	Yb	Tm	475,698,800	[19, 43]
LaF <sub>3</sub>	Yb	Ho	541,643	[44, 45]
YF <sub>3</sub>	Yb	Er	411,526,552,664	[44, 46]
YF <sub>3</sub>	Yb	Tm	347,636,454,477	[47, 48]
LuF <sub>3</sub>	Yb	Tm	481	[49, 50]
NaYF <sub>4</sub>	Yb	Er	525,547,660	[27, 51, 52]
NaYF <sub>4</sub>	Yb	Tm	450,476,800	[53, 54]
NaYF <sub>4</sub>	Yb	Ho	541	[55]
LiYF <sub>4</sub>	Yb	Tm	361,450,479,647	[56]
NaGdF <sub>4</sub>	Yb	Ho	541,647,751	[57]
KY <sub>3</sub> F <sub>10</sub>	Yb	Er	522,545,656	[58, 59]
KGd <sub>2</sub> F <sub>7</sub>	Yb	Er	525,552,666	[59]
BaYF <sub>5</sub>	Yb	Tm	475,650,800	[60–62]

**Table 3.**  
 UCNF detailed with NIR excitation for fluorides.

does not necessarily guarantee high luminescence. The energy transfer process between ions is governed by several factors, such as the crystal structure of the host lattice, which determines the distance and spatial arrangement of the doping ions. Therefore, the host lattice should have a low phonon energy and a close lattice match with the dopant ions. These characteristics help minimize non-radiative losses and maximize radiative emission [63–65]. The successful utilization of UCNPs in biomedicine relies on careful selection of nanoparticles, considering factors such as size, shape, ease of functionalization, and tendency to agglomerate, among others. These factors are crucial for ensuring optimal performance and compatibility with biomedical applications.

A wide variety of luminescent nanoparticles (NPs) can be utilized for biomedical applications, distinguished by the chemical nature of their host lattice. Different systems include sulfides (ZnS, CaS, BaS, SrS) [63], oxides (ZnO, Fe<sub>3</sub>O<sub>4</sub>) [64], and lanthanides oxides [65]. These systems exhibit strong emission spectra ranging from 450 to 700 nm, achieved by incorporating trivalent lanthanide ions such as Yb, Er, and Tm. More specific details regarding these combinations can be found in **Table 1**.

**Table 2** highlights less commonly used host lattices, including phosphates, molybdates, tungstates, gallates, and vanadates. It is worth noting that oxides, in general, tend to exhibit greater stability. However, molybdate hosts have a small optical band gap, which can result in thermal quenching, limiting their suitability in certain applications. **Table 3** focuses on fluorides, such as CaF [66] and lanthanides fluorides [67]. These types of host lattices are popular due to their advantageous properties. However, one disadvantage is that it can be more challenging to obtain nanocrystals with sizes smaller than 50 nm using these host lattices.

Several of the mentioned systems offer not only luminescence but also additional exciting features. For instance, Fe<sub>3</sub>O<sub>4</sub> nanoparticles exhibit magnetic

properties [64], making them highly valuable for more efficient targeting of cancer cells. Gold nanoparticles supported on  $\text{TiO}_2$  show a photo-thermal response [68], allowing for applications in targeted photothermal therapy.  $\text{CeO}_2$  nanoparticles exhibit antimicrobial behavior providing potential applications in combating microbial infections [69]. Additionally, inorganic nanoparticles with high surface area and porosity, such as those based on certain materials, can improve the ability to carry drugs [70]. The chemical nature of inorganic nanoparticles directly influences their functionalization, enabling specific modifications for desired applications. Furthermore, the crystal properties of these inorganic nanoparticles are crucial for understanding and controlling their luminescent behavior in synthesized materials. A comprehensive understanding of both the chemical and crystal properties is vital in harnessing the full potential of these materials for various applications.

## **2.1 Synthesis of the nanoparticles**

Achieving high-quality UCNPs requires careful control over their composition, size, shape, and crystalline phase. The synthesis process plays a critical role in attaining these desired characteristics. The most popular synthesis methods for UCNPs are based on the “bottom-up” approach, commonly known as wet chemistry. This approach involves chemical reactions in a liquid solution to form nanocrystals. Wet chemistry methods offer advantages in producing uniform nanocrystals, allowing for precise control over particle size and minimizing agglomeration.

By employing the bottom-up approach, researchers can carefully manipulate reaction parameters such as precursor concentrations, reaction time, temperature, and choice of solvent to achieve the desired properties of UCNPs. This control over the synthesis process enables the production of UCNPs with tailored characteristics, facilitating subsequent functionalization and integration into specific applications [71]. The LNPs, in general, can be synthesized in the same way, no matter if they are DCNP or UCNP.

### *2.1.1 Sol-gel method*

The sol-gel process is a synthesis method that involves the hydrolysis and polycondensation of metal alkoxides (or halides) as precursors. This process is conducted at relatively low temperatures; however, to improve the crystallinity of the resulting nanomaterials, calcination at high temperatures is often required. The high luminescence efficiency of the nanoparticles can be attributed to this post-calcination step.

Several researchers have explored the sol-gel process for the synthesis of luminescent nanoparticles. For example, Taxak [72] utilized tartaric acid-assisted  $\text{Y}_2\text{O}_3:\text{Eu}^{3+}$  DCNPs using this method. Talane et al. [73] prepared  $\text{TiO}_2:\text{Er}^{3+}$  UCNPs through the sol-gel process. Chavez et al. [10] also employed the sol-gel method to produce tartaric acid-assisted UCNPs with two different host lattices:  $\text{Y}_2\text{O}_3$  and  $\text{Gd}_2\text{O}_3$ . In their study,  $\text{Y}(\text{NO}_3)_3$  and  $\text{Gd}(\text{NO}_3)_3$  were used as precursors, along with doping precursors  $\text{Yb}(\text{NO}_3)_3$  and  $\text{Er}(\text{NO}_3)_3$ . The  $\text{Y}_2\text{O}_3$  nanoparticles required higher calcination temperatures of up to  $1200^\circ\text{C}$ .

However, one drawback of the sol-gel process is the need for higher calcination temperatures, which can be a limitation in terms of energy requirements and potential impact on the material or substrate being used.

### 2.1.2 Thermal decomposition

Thermal decomposition is another synthesis method that can yield high-quality UCNPs with controlled size and desirable shapes [74]. This method involves two steps. In the first step, organic precursors are dissolved in high-boiling point organic solvents along with surfactants. In the second step, the precursors are decomposed at elevated temperatures. Organic acid compounds such as trifluoroacetate, acetoacetate, and oleate, among others, can serve as precursors in this process.

Boyer et al. [75] demonstrated the synthesis of NaYF<sub>4</sub> UCNPs co-doped with Yb/Er or Yb/Tm using thermal decomposition with metal trifluoroacetate precursors in the presence of oleic acid and octadecene. Oleic acid not only acted as a solvent but also as a passivating ligand to prevent agglomeration of the UCNPs.

It is important to note that there are certain disadvantages associated with this method. The use of toxic or expensive precursors can be a limitation in some cases, and it is necessary to handle them with care. Additionally, the cost of the process itself can be relatively high due to the requirements of elevated temperatures and the use of specialized equipment.

### 2.1.3 Hydrothermal method

The hydrothermal method is a widely used technique to produce luminescent nanoparticles with high crystallinity. This method involves using solvents, either hydrophilic or lyophilic, at high temperatures inside autoclaves to create autogenic high pressure. The elevated temperature and pressure promote the solubility and reordering of precursors, resulting in the formation of high-quality nanoparticles.

The hydrothermal method typically operates at relatively low reaction temperatures, allowing for precise control over the morphology of the nanoparticles. Lin et al. developed an effective method for producing nanoparticles with different shapes based on rare earth elements. They discovered that the addition of trisodium citrate as an organic additive, the choice of fluoride source, and the pH value of the initial solution greatly influenced the shape of the nanoparticles [76].

However, it is worth noting that there are limitations to this method. Nanoparticles produced via hydrothermal synthesis generally cannot be smaller than 10 nm in size. Additionally, some hydrothermal reactions may require prolonged heating periods to complete the synthesis.

### 2.1.4 Coprecipitation method

Coprecipitation is indeed a commonly used method for synthesizing ultrasmall NPs. It offers advantages such as simplicity, low cost, and does not require complex equipment or procedures. In coprecipitation, the simultaneous precipitation of multiple components allows for the formation of nanoparticles.

Typically, a subsequent heat treatment step is required to improve the crystallinity of the synthesized NPs. This heat treatment is commonly performed at temperatures ranging between 400 and 600°C.

In a study by Yi et al. [77], they synthesized LaF<sub>3</sub>:Yb<sup>3+</sup>, Er<sup>3+</sup>/Ho<sup>3+</sup>/Tm<sup>3+</sup> UCNPs with a very small particle size of 5.4 ± 0.9 nm. They utilized ethylenediamine tetraacetic acid as a chelating reagent in the coprecipitation process. Overall, coprecipitation is a versatile and straightforward method for producing ultrasmall nanoparticles, and subsequent heat treatment can enhance their crystallinity and properties.



### 2.1.5 Combustion synthesis

Combustion synthesis is a highly exothermic reaction method, typically performed within a temperature range of 500 to 3000°C. Despite its tendency to cause agglomeration during the process, several authors have successfully utilized this method for the synthesis of upconversion nanoparticles (UCNPs).

In a study by Pendey et al. [78],  $Y_2O_3$  co-doped with  $Ho^{3+}$  and  $Yb^{3+}$  was synthesized using combustion synthesis, resulting in high green emissions. Although agglomeration can occur during combustion synthesis, these methods remain widely used for the production of UCNPs in biomedical applications. Researchers often personalize and refine their synthesis methods to achieve spheroidal nanoparticles with reduced agglomeration. Surfactants are sometimes incorporated into the process to improve the quality and shape of the nanoparticles. These efforts aim to enhance the overall performance and applicability of the synthesized UCNPs.

The following **Table 4** presents a summary of the various methods explained. These are not the only methods that may exist; we are presenting the most common ones used by researchers.

## 2.2 Functionalization of nanoparticles

The functionalization of nanoparticles plays a crucial role in the development of materials for cancer treatment. This process involves modifying the surface of the nanoparticles to make them compatible with biological systems and enable specific targeting of cancer cells.

To achieve this, the nanoparticles are made biocompatible by attaching a chemical group that facilitates the binding of various ligands. These ligands are designed to specifically bind to overexpressed receptors on cancer cells, such as the folate receptor (FR), transferrin receptor (TfR), epidermal growth factor receptor (EGFR),

Method	Advantages	Disadvantages	References
Sol-gel	It is performed at relatively low temperatures	High calcination temperatures	[72, 73]
Thermal decomposition	It can result in high-quality UCNPs with precise control over their size and shapes	The utilization of toxic or costly precursors entails careful handling precautions and incurs elevated expenses	[74, 75]
Hydrothermal	It can produce high crystallinity	LNPs cannot be smaller than 10 nm in size. Certain hydrothermal reactions may necessitate prolonged heating periods to achieve complete synthesis	[76]
Coprecipitation	Simple, low cost, and does not require complex equipment	Heat treatment is required to improve the crystallinity	[77]
Combustion synthesis	Fast and highly exothermic reaction method	It has a tendency to cause agglomeration of the LNPs during the process	[78]

**Table 4.**  
*Synthesis of LNPs.*

G-protein coupled receptor (GPCR), low-density lipoprotein receptor (LDLR), and lectins, among others. **Figure 1** illustrates the basic concept of UCNPs and the functionalization process that enables them to target specific cells. The first step involves the synthesis of UCNPs using the upconversion process. Then, the nanoparticles are functionalized to make them biocompatible and capable of binding to specific ligands. Finally, the functionalized UCNPs can bind to the desired cancer cells, allowing for targeted delivery or imaging applications. This functionalization process is essential for enhancing the selectivity and effectiveness of cancer treatment by enabling nanoparticles to specifically interact with cancer cells while minimizing interactions with healthy cells.

**Figure 1** illustrates the fundamental procedure required to functionalize UCNPs for targeting specific cells. For example, folic acid (FA) is one of the chemical groups commonly used to modify the surface of nanoparticles due to the overexpression of folate receptors (FR) in many human cancer cells [79, 80]. The presence of FR makes folic acid an attractive ligand for targeted drug delivery to cancer cells.

Polyethylene glycol (PEG) is another widely used chemical group for nanoparticle functionalization. PEG functionalization enhances the biocompatibility of nanoparticles due to the hydrophilic nature of the PEG molecule [81]. The presence of PEG on the nanoparticle surface reduces non-specific interactions and helps to increase circulation time in the body.

The size of nanoparticles also plays a significant role in their biodistribution and targeting efficiency. Cheng et al. [82] conducted research on *in vivo* targeted drug delivery using nanoparticles for prostate tumors. They found that the nanoparticle size had a significant impact on the biodistribution of targeted and non-targeted nanoparticles in an organ-specific manner. This study highlights the importance of nanoparticle size in achieving effective targeted drug delivery.

Overall, the functionalization of nanoparticles with chemical groups like FA and PEG enables targeted drug delivery and enhances their biocompatibility, making them suitable for biomedical applications. Manson et al. [83] conducted a study on

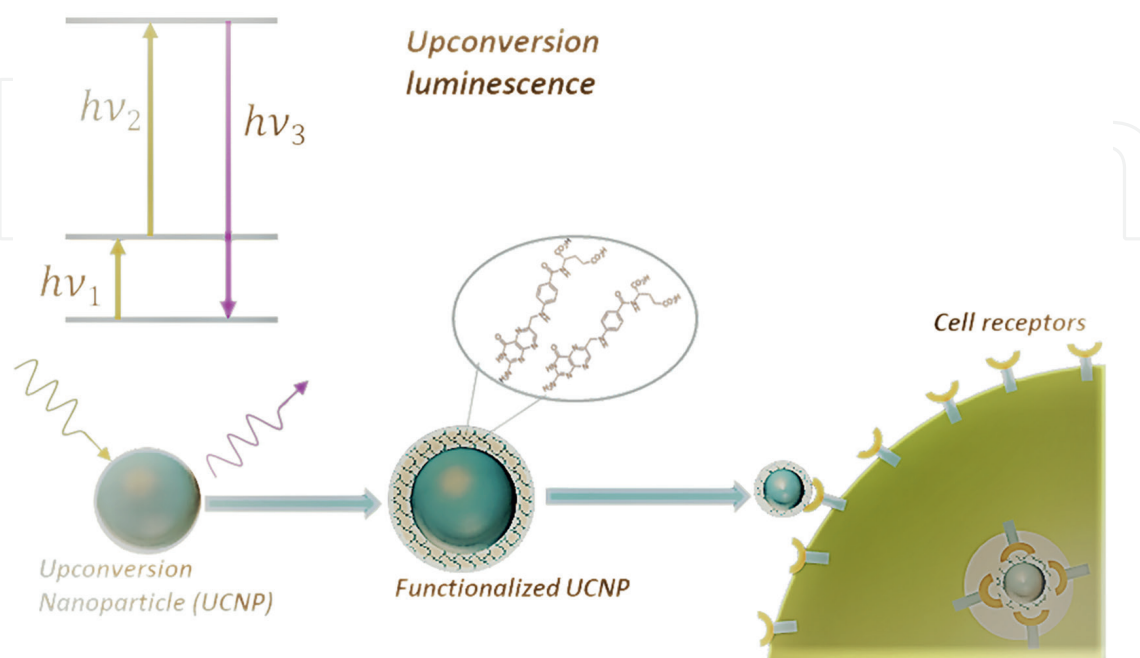


**Figure 1.** Image shows the basic procedure needed to functionalize UCNPs to target specific cells.

the capping density of PEG on gold nanoparticles (AuNPs) and its impact on the surface properties of the nanoparticles in various solutions. The study revealed that the PEG-coated nanoparticles exhibited significantly increased stability, facilitating their production in different media. This enhanced stability is essential for ensuring the nanoparticles' functionality and performance in various applications.

In another study by Maldiney et al. [84], the effect of optical detection using PEGylated lanthanide-doped luminescent nanoparticles (NPs) emitting in the near-infrared (NIR) window was investigated in healthy and tumor-bearing mice. The researchers found that the tissue distribution of the nanoparticles was highly dependent on the surface coverage of PEG as well as the core diameter of the nanoparticles. They concluded that PEG coverage led to a homogeneous and well-distributed presence of highly stable particles throughout the animal, highlighting the importance of PEGylation for achieving effective and stable distribution of nanoparticles in biological systems.

These studies emphasize the significance of PEG functionalization in enhancing the stability, production, and distribution of nanoparticles in various media and biological systems. PEGylation plays a crucial role in ensuring the biocompatibility, stability, and targeted delivery capabilities of nanoparticles, making them valuable tools in biomedical applications.

Silica (SiO<sub>2</sub>) coating is another effective method for functionalizing nanoparticles. Wang et al. [41] conducted a study on UCNPs coated with silica (LaF<sub>3</sub>: Yb, Er@SiO<sub>2</sub>) in zebrafish embryos. They found that a high dose of fluoride UCNPs (> 200 µg/mL) could lead to malformations, delayed hatching rate, and impaired embryonic and larval development. The study highlights the importance of carefully considering the dosage and potential toxicity of nanoparticles, even when they are functionalized with silica coatings. While functionalization can improve the biocompatibility and stability of nanoparticles, it is crucial to ensure that the dosage used does not have adverse effects on biological systems. This underscores the importance of conducting thorough toxicity assessments and dose optimization studies when utilizing functionalized nanoparticles in biological applications.

Polyethyleneimine (PEI) is indeed a commonly used method for functionalizing nanoparticles. When combined with small-interfering RNA (siRNA), it offers a powerful strategy for targeted therapy in various diseases. siRNA is a synthetic double-stranded RNA molecule consisting of approximately 21 nucleotides. It is designed to trigger a specific and sequential degradation of target mRNA through the RNA interference (RNAi) mechanism. This functionalization approach provides a potential strategy for silencing mutated or defective genes that contribute to various human diseases. Buchman et al. [85] developed a new method for the covalent attachment of PEI for siRNA delivery. They demonstrated that nanoparticles functionalized with this approach exhibited thermodynamic stability, efficient binding to siRNA molecules, and sustained silencing effects even after storage for at least 1 year. This research highlights the potential of PEI-based functionalization for effective and long-term delivery of siRNA, enabling targeted gene silencing for therapeutic purposes.

Polyvinylpyrrolidone (PVP) and polyacrylic acid (PAA) are indeed commonly used for the functionalization of nanoparticles. Wang et al. conducted research on the functionalization of upconversion nanoparticles (UCNPs) NaYF<sub>4</sub>:Yb, Er with various coatings including PEG, PVP, PAA, and PEI with -COOH and -NH<sub>2</sub> groups [27, 53]. These functionalized nanoparticles have shown great potential for applications in biomedicine. In another study by Liu et al. [86], PAA functionalization of UCNPs

with -COOH and -NH<sub>2</sub> groups was employed for immunoassays. The functionalized UCNPs demonstrated high sensitivity for biosensing and exhibited high contrast for bioimaging applications.

The use of PVP, PAA, and other functionalization agents allows for the modification of nanoparticles' surface properties and facilitates their interactions with biological systems. These functionalized nanoparticles have shown promise in various biomedical applications, including drug delivery, biosensing, and bioimaging, due to their enhanced biocompatibility and tailored surface properties.

In the study by Yang [87], NaREF<sub>4</sub> nanoparticles (NPs) co-doped with Nd–Lu and Y were obtained using a phase-transition process. This process involved the use of sodium dodecylsulfate (SDS) as an amphiphilic surfactant within the same reaction system. As a result, hollow-structured NPs were generated in situ. These hollow-structured NPs have unique properties and can be easily synthesized using electron-beam lithography on solid NPs. They exhibited good biocompatibility, making them suitable for biomedical applications. In the study, the NPs were tested for drug storage and delivery, as well as for cancer therapy drug carrier studies. The hollow structure of these NPs provides opportunities for drug encapsulation, controlled release, and targeted delivery. This research contributes to the exploration of novel nanomaterials for drug delivery systems and holds potential for advancements in cancer therapy.

Folic acid is an essential vitamin involved in various metabolic reactions, including the synthesis of purine and pyrimidine bases. Due to the high demand for these bases in rapidly proliferating tumor cells, FA is required in larger quantities by cancer cells. Moreover, several types of cancer cells, such as ovarian and uterine cancer cells, exhibit overexpression of folate receptors at higher rates compared to normal cells. This makes FA an excellent targeting molecule for cancer cells in both in vitro and in vivo applications.

Suvorov et al. reported a non-invasive method using FA-functionalized nanoparticles (NPs) conjugated with photosensitizers (PS) for photodynamic therapy (PDT) of cancer. In this approach, the PS is taken up by the tumor, and upon local irradiation with light of a specific wavelength, active oxygen forms, including singlet oxygen, are generated. These active oxygen species cause cell death in the tumor cells and surrounding tissue, leading to therapeutic effects [88, 89]. Overall, the use of FA-functionalized NPs holds great promise for targeted drug delivery and therapeutic applications, offering the potential for enhanced cancer treatment outcomes while minimizing off-target effects on healthy cells.

In a study conducted by Xie et al. [90], the self-assembly abilities of Brome mosaic virus (BMV) capsid proteins were investigated in the aprotic polar solvent dimethyl sulfoxide (DMSO), which differs from the typical aqueous buffers used in previous studies. The researchers observed that the BMV capsid proteins retained their ability to self-assemble in DMSO, enabling the encapsulation of nanoparticles and dye molecules that are more soluble in organic solvents, such as β-NaYF<sub>4</sub>-based UCNPs and BODIPY dye. Surprisingly, the assembly process demonstrated robustness and adaptability across a wide range of DMSO concentrations. Particularly interesting was the finding that cargos with poor stability in aqueous solutions could be easily encapsulated at high DMSO concentrations and subsequently transferred to aqueous solvents, where they maintained stability and functionality for an extended period of several months. This study underscores the potential of utilizing alternative solvents, such as DMSO, for virus assembly and encapsulation, opening up new avenues for the development of functional nanomaterials.

Ensuring the biocompatibility of functionalized NPs is a critical consideration for their use in biomedical applications. Additionally, minimizing particle aggregation is important to maintain the circulation of NPs within the human body and their efficient delivery to targeted cancer cells. Numerous studies have focused on achieving efficient functionalization of NPs, resulting in successful uptake of NPs by cells and improved biocompatibility.

Indeed, the coating and functionalization of nanoparticles can pose challenges such as agglomeration. To overcome this issue, surfactants are commonly employed to reduce agglomeration and achieve adequate coating, ensuring the biocompatibility of the nanoparticles and facilitating their successful penetration into cells. Surfactants act by stabilizing the nanoparticles, preventing them from clumping together, and promoting their dispersion.

In addition to surfactants, mechanical methods such as sonication are often utilized to enhance the dispersion of nanoparticles before functionalization. Sonication involves the application of high-frequency sound waves, which create cavitation bubbles that implode, exerting shear forces and promoting the breakup of particle aggregates. This mechanical treatment helps to disperse the nanoparticles more effectively, enhancing their stability and facilitating subsequent functionalization processes.

By utilizing surfactants and employing mechanical methods like sonication, researchers aim to minimize agglomeration and achieve better dispersion and coating of nanoparticles. These strategies contribute to improving the biocompatibility of nanoparticles and their ability to interact with target cells, ultimately enhancing their potential for biomedical applications.

### 3. Bioimaging with nanomaterials

Bioimaging is a powerful technique that enables the visualization of various biological structures and their functions with high resolution. It offers a level of detail that surpasses traditional imaging methods such as X-ray or magnetic resonance imaging (MRI). Bioimaging can be conducted on living organisms, providing insights into dynamic processes and interactions within the body, or on *in vitro* cell cultures to study cellular behaviors and molecular processes.

In the context of *in vivo* bioimaging, it allows researchers to non-invasively observe and track biological phenomena in real time within living animals. This includes imaging specific tissues or organs, studying the progression of diseases, monitoring therapeutic responses, and exploring the biodistribution and pharmacokinetics of drugs or nanoparticles.

For *in vitro* bioimaging, cell cultures can be examined under various microscopy techniques to investigate cellular structures, protein localization, gene expression, and cellular responses to external stimuli. This enables researchers to gain a deeper understanding of cellular processes, cell-cell interactions, and the effects of various interventions.

Bioimaging techniques encompass a wide range of methods, including fluorescence microscopy, confocal microscopy, multiphoton microscopy, positron emission tomography (PET), single-photon emission computed tomography (SPECT), and more. Each technique offers specific advantages and capabilities, allowing researchers to tailor their imaging approach to the specific biological question or experimental setup [91].

In summary, bioimaging plays a crucial role in advancing our understanding of biological systems, both *in vivo* and *in vitro*. It provides detailed visualizations of

structures and processes, enabling researchers to unravel the complexities of biology and contribute to advancements in fields such as medicine, drug development, and basic biological research [87, 92, 93].

### 3.1 *In vitro* cellular imaging

*In vitro* cellular imaging provides an intuitive visualization of physiological processes and interactions among cells, proteins, and molecules [94]. Researchers have utilized laser scanning upconversion luminescence (UCL) microscopy systems, such as the one developed by Yu and colleagues [95], for cellular imaging with UCNPs. The unique anti-Stokes emission modality of UCNPs, which differs from single-photon and two-photon emissions, presents a challenge for cellular imaging due to out-of-focus upconversion emissions. To overcome this, a reverse excitation dichroic mirror and confocal pinhole technique were employed in the microscopy system.

The common incubation concentration of UCNPs with cells for cellular imaging typically ranges between 10 and 200  $\mu\text{g}/\text{mL}$ . Hu et al. developed cellular imaging using PEG-OH  $\text{LaF}_3:\text{Yb}, \text{Ho}$  UCNPs [45]. They achieved good cell membrane permeability with KB cells, enabling the UCNPs to serve as bioimaging probes. The UCNPs exhibited strong intracellular upconversion emissions within the wavelength range of 545 to 645 nm.

The effect of coated UCNPs on cellular uptake and imaging has been studied by various researchers. Jin et al. [96] investigated cubic  $\text{NaYF}_4:\text{Yb}, \text{Er}/\text{Tm}$  UCNPs coated with different polymers for cellular imaging. They synthesized PVP-UCNPs, PAA-UCNPs, and PEI-UCNPs using polyvinylpyrrolidone (PVP), polyacrylic acid (PAA), and polyethyleneimine (PEI), respectively. Based on imaging results, they found that PEI-UCNPs exhibited more effective intracellular uptake. This finding aligns with a report by Tsang et al. who obtained similar results in their study with HeLa cells. The significant cell uptake of PEI-UCNPs is attributed to the electrostatic attraction between the amino groups ( $-\text{NH}_2$ ) on PEI and the cell membrane [97].

These studies highlight the importance of surface coatings and their impact on cellular uptake and imaging performance of UCNPs. The choice of coating material can significantly influence the cellular uptake efficiency, allowing for enhanced imaging capabilities and better understanding of cellular processes.

**Figure 2** depicts an example of how the *in vitro* cellular imaging appears with confocal microscopy of cervical (HeLa) and breast (MCF-7) adenocarcinoma cell lines [98].

### 3.2 *In vivo* tumor imaging

*In vivo* tumor imaging is crucial for understanding the mechanism of drug function. To address the limitations of UCNP applicability in *in vivo* imaging, researchers have explored the use of UCNPs doped with  $\text{Tm}^{3+}$  and  $\text{Er}^{3+}$  ions. These UCNPs offer better performance for deep tissue imaging. De la Rosa et al. highlighted that the optimal excitation wavelength for UCNP, around 980 nm, coincides with the absorption band of water, leading to potential tissue heating. However, when UCNP is a Raman micro-spectroscopy excited at 915 nm wavelength, optical excitation of  $\text{Yb}^{3+}$  can still occur without interference from water [99–101].

UCNPs have several advantages for *in vivo* imaging. They can be designed to emit fluorescence under specific excitation wavelengths, allowing for targeted activation and detection of disease-specific tissues. Xiong et al. [102] functionalized UCNPs with FA and demonstrated significant upconversion luminescence signals in mice tumors after intravenous injection.

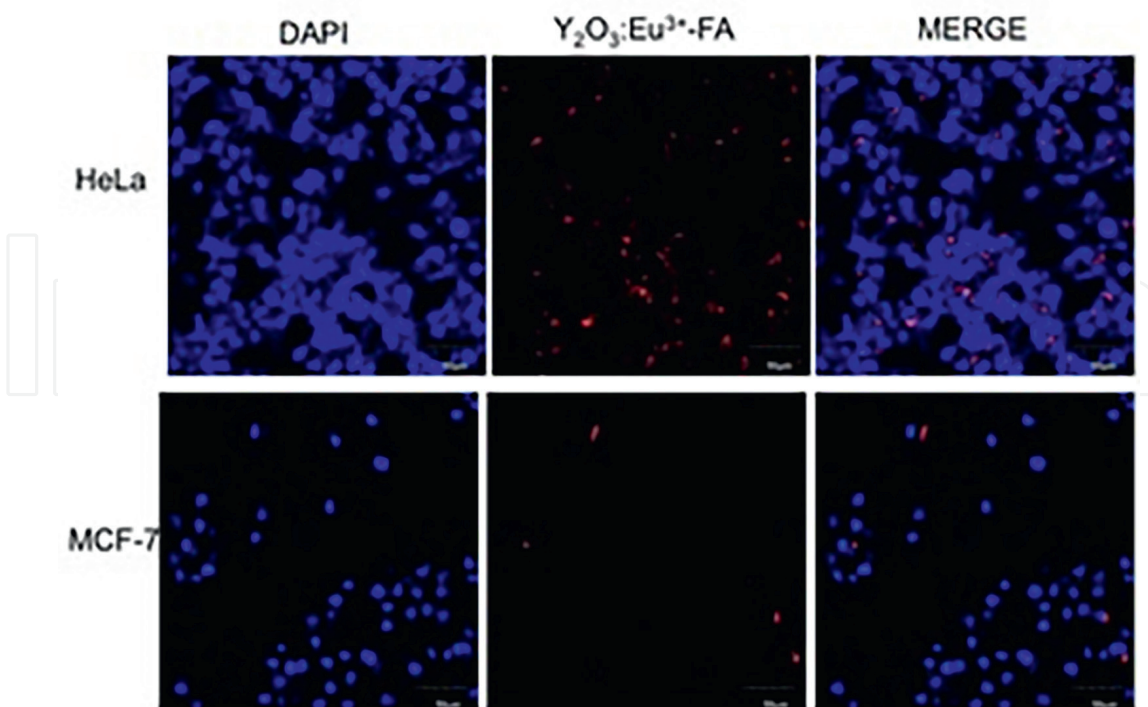


**Figure 2.** Cellular localization of fluorescence  $Y_2O_3:Eu^{3+}$ -FA nanoparticles in cancer cells. Cervical (HeLa) and breast (MCF-7) adenocarcinoma cell lines incubated with LNPs-FA (red). DAPI depicts nuclear staining in blue [98].

Gadolinium-based UCNPs, where  $Gd^{3+}$  ions are incorporated into the host lattice, offer both magnetic resonance imaging (MRI) and luminescence contrast, enabling multimodal imaging. Similarly, UCNP  $NaLuF_4: Yb, Tm$  can act as dual contrast agents for computerized tomography (CT) and upconversion luminescence in lymphatic imaging. Zeng et al. [103] employed tri-modal imaging combining radionuclide labeling with MRI- or CT-capable UCNP PEG- $BaGdF_5: Yb/Er$  for in vivo tumor diagnosis.

One challenge of UCNP is their relatively low brightness, which can be attributed to narrow excitation bands, low absorption cross-sections, and surface-induced quenching effects. Researchers have addressed these issues by manipulating the host structure through the addition of dopant ions or by modifying the NP surface with molecules or materials that enhance light absorption, such as dyes and plasmonic materials [4]. High-resolution in vivo imaging is desirable for achieving detailed spatial resolution. Hilderbrand et al. [104] studied the use of  $Y_2O_3: Yb, Er$  UCNPs for in vivo vascular imaging in mice, demonstrating clear images of vessels and long circulation of UCNPs for up to 2 hours post-injection.

UCNPs offer significant advantages in bioimaging for both *in vivo* and *in vitro* applications. They provide tissue autofluorescence-free imaging and improved spatial resolution due to reduced scattering at longer wavelengths. Ongoing research efforts aim to address the challenges and improve the utilization of UCNPs in bioimaging [105].

## 4. Cellular uptake and toxicology of nanoparticles

### 4.1 Toxicology of nanoparticles

With the increased use of UCNPs, concerns have been raised regarding their potential impact on human health and biological systems. Consequently, numerous

studies have been conducted to assess the uptake of UCNPs into cells or tissues and evaluate their potential toxicity.

Several assays are commonly employed to assess the cytotoxicity of NPs in cells, such as the MTT assay. This assay measures cell viability by assessing the ability of cells to convert the yellow tetrazolium salt (MTT) into a purple formazan product through mitochondrial activity. Positive and negative controls are used to determine total cell death and cell survival, respectively. Cells are incubated with UCNPs at various concentrations for specific incubation periods, and the cell viability is then measured using an ELISA reader or a similar method that quantifies the color change [106]. For example, Shan et al. [107] performed a biofunctionalization study on NaYF<sub>4</sub>: Yb, Er UCNPs. They coated the UCNPs with a layer of SiO<sub>2</sub> and introduced amino and carboxyl groups. The UCNPs were incubated with cells at a concentration of 1 mg/mL for 9 days. Their results showed that UCNPs functionalized with amino groups exhibited 96.2% cell viability, while those functionalized with carboxyl groups exhibited 92.8% cell viability, indicating minimal toxicity.

In addition to the MTT assay, other assays are employed to evaluate potential toxic effects of UCNPs, such as assessing reactive oxygen species (ROS) generation, apoptosis, necrosis cell death assays, and genotoxicity using the comet assay. These assays provide valuable insights into the potential biological impact of UCNPs and help assess their safety profile.

Reactive oxygen species (ROS) are highly reactive molecules that can cause oxidative damage to biological macromolecules, leading to functional impairment. ROS are generated during cellular respiration and play important roles in various physiological processes, including cell development, differentiation, oxidative stress, and cell death. The formation of ROS by nanoparticles is one of the mechanisms through which nanoparticles can exert toxicity [108].

Many studies have investigated the generation of ROS by nanoparticles as a means to evaluate their biocompatibility. One commonly used method for detecting ROS and reactive nitrogen species (RNS) is the reaction of 2,2,6,6-tetramethylpiperidine (TEMP) with superoxide radicals (O<sup>2-</sup>), which can be detected using X-band electron paramagnetic resonance (EPR). However, this method can be costly compared to using fluorescent probe molecules. Another limitation of the EPR method is its inability to react with a wide range of reactive species. In addition to the EPR method, there are other techniques available for detecting and quantifying ROS, such as fluorescence-based probes. These probes can selectively react with specific ROS species, providing a more comprehensive assessment of ROS generation and their potential effects [109].

Overall, investigating the generation of ROS by nanoparticles is an important aspect of assessing their toxicity and biocompatibility. The choice of detection method depends on various factors, including the specific ROS species of interest, the sensitivity required, and the cost-effectiveness of the method.

Flow cytometry is a powerful technique for analyzing cell health and assessing compound cytotoxicity. It provides a detailed and comprehensive analysis of various cellular parameters, including cell viability, apoptosis, and necrosis. Flow cytometry utilizes fluorescently labeled probes and antibodies to measure specific cellular markers and characteristics [110].

Cell death can be assessed by flow cytometry through the detection of apoptosis and necrosis markers. Apoptosis is a programmed cell death process characterized by specific morphological and biochemical changes, such as membrane blebbing, DNA fragmentation, and caspase activation. Necrosis, on the other hand, is a form of cell



death typically associated with cellular damage and disruption, leading to the release of cellular contents. To discriminate between apoptotic and necrotic cell death, specific fluorescent markers can be used. For example, Annexin V is commonly used to detect early apoptotic cells by binding to phosphatidylserine exposed on the outer leaflet of the plasma membrane. Propidium iodide (PI) or 7-aminoactinomycin D (7-AAD) can be used to assess necrotic cells by detecting the loss of plasma membrane integrity [111–113].

In addition to flow cytometry, Raman micro-spectroscopy has emerged as a non-invasive and label-free technique for studying cell death processes. Raman spectroscopy measures the vibrational frequencies of molecular bonds, providing information about the biochemical composition and structural changes within cells. By analyzing Raman spectral shifts associated with specific cellular components, such as proteins, lipids, and nucleic acids, researchers can differentiate between different modes of cell death, including apoptosis and necrosis [114, 115].

The study conducted by Brauchle and et al. [116] aimed to investigate induced apoptosis and heat-triggered necrosis in Saos-2 and SW-1353 cells using Raman micro-spectroscopy at room temperature. Raman micro-spectroscopy is a label-free technique that allows for the analysis of biochemical composition and structural changes within cells. In the study, the researchers exposed the cells to specific stimuli to induce apoptosis and heat-triggered necrosis. They then performed Raman micro-spectroscopy measurements on the cells to analyze the resulting spectral shifts associated with these different cell death processes. By examining the Raman spectra of the cells, the researchers were able to identify distinct biochemical signatures associated with apoptosis and necrosis. Apoptotic cells exhibited characteristic spectral changes, such as alterations in protein conformation and nucleic acid content. On the other hand, heat-triggered necrotic cells displayed different spectral features, including changes in lipid composition and membrane integrity. The use of Raman micro-spectroscopy in this study allowed for the discrimination and identification of different modes of cell death, providing valuable insights into the biochemical changes associated with apoptosis and necrosis. This non-invasive and label-free technique offers the advantage of studying complex cell-death-related processes in a continuous and real-time manner, without the need for exogenous labels or probes. Overall, the study by Brauchle and colleagues demonstrated the utility of Raman micro-spectroscopy in elucidating the biochemical characteristics and dynamics of cell death processes, contributing to a deeper understanding of these important biological events.

The combination of Raman micro-spectroscopy with other techniques, such as fluorescent microscopy, allows for a more comprehensive understanding of complex cell-death-related processes. This approach enables continuous and non-invasive monitoring of cell death events, providing valuable insights into the underlying mechanisms and dynamics of cell response to cytotoxic stimuli.

The genotoxicity testing is crucial for evaluating the potential harmful effects of chemicals on the genetic material of cells. The comet assay, also known as the single-cell gel electrophoresis assay, is a widely used technique to assess DNA damage and genotoxicity. It involves exposing cells to a test substance and then subjecting them to electrophoresis, which causes fragmented DNA to migrate away from the nucleus, creating a “comet” shape. The comet assay allows researchers to measure various types of DNA damage, including single-strand breaks, double-strand breaks, and alkali-labile sites. By comparing the extent of DNA damage in treated cells with untreated control cells, the genotoxic potential of a chemical can be determined. The assay can be performed on different cell types, including in vitro cultured cells or even in vivo tissues [117–119].

PDT is a treatment that utilizes non-toxic dyes called photosensitizers (PS) and harmless visible light to generate reactive oxygen species (ROS), by damaging biomolecules and killing cells. While PDT has primarily been developed as a cancer therapy, it can also be used as an antimicrobial approach for localized infections. However, the limited tissue penetration of the longest wavelength used for exciting PS poses a challenge. To address this, Hamblin [120] investigated the use of UCNPs to enable the use of deeper-penetrating near-infrared light for PDT. Specifically, NaYF<sub>4</sub> nanoparticles doped with Yb<sup>3+</sup> and Er<sup>3+</sup> or Tm<sup>3+</sup> and Er<sup>3+</sup> have been attached to PS, allowing NIR light energy to be transduced into ROS, leading to cell killing and tumor regression. Various advancements have been made, including the use of dye-sensitized UCNPs, UCNPs coupled with PS, and the exploration of synergistic drug molecules or techniques. Additionally, the combination of upconversion PDT with different bioimaging modalities has shown promise. However, further research is needed to optimize the drug-delivery capabilities of UCNPs, improve quantum yields, enable intravenous injection and tumor targeting, and ensure safety at required doses before potential clinical applications can be realized.

Nigoghossian et al. [121] focused on evaluating the cytotoxicity, genotoxicity, and mutagenicity of UCNPs incorporated into a 3D-printed composite scaffold with upconversion luminescence for potential biomedical applications. Their system combined the polymer PCL, UCNPs-apatite, and a photosensitizer for PDT in stimulating bone repair. The authors used low concentrations of lanthanide elements in their study and reported no toxicological effects, indicating that the UCNPs incorporated into the scaffold did not induce significant cytotoxicity, genotoxicity, or mutagenicity.

Similarly, Doronkina et al. [122] worked with NaYF<sub>4</sub>: Er,Yb UCNPs functionalized with NH<sub>2</sub>-FA and studied erythrocyte aggregation, genotoxicity, and DNA damage. Their findings indicated no genotoxicity or DNA damage associated with the UCNPs. It is important to note that specific results and conclusions may vary depending on the experimental conditions, nanoparticle characteristics, and cell types used in each study. Each study contributes to our understanding of the potential effects and safety profile of UCNPs in various biological systems.

**Table 5** presents the cell viability and surface coating of various UCNP studied by different authors across different types of cells.

Most of the authors reported more than 90% cell viability with functionalized UCNPs, thereby confirming their biocompatibility with the cells under study. These authors utilized several of the techniques mentioned earlier to assess cell viability.

## 4.2 Cellular uptake of nanoparticles

To corroborate the cellular uptake of NPs for in vitro applications, several techniques can be employed to evaluate it. These techniques provide insights into the internalization and localization of NPs within cells. Some commonly used techniques include:

- **Flow cytometry:** Flow cytometry allows for the quantitative analysis of NPs uptake by cells. It involves labeling NPs with fluorescent dyes or using fluorescently labeled antibodies to detect and quantify the internalized NPs in individual cells. This technique provides information about the percentage of cells that have taken up NPs and can also assess the uptake efficiency.

Host lattice	Sensitizer/ Activator	Surface coating/ Modification	Cell type	Cell viability	Reference(s)
NaYF <sub>4</sub>	Yb, Er	PEI-FA	BMS cells 1	~100% >90%	[123]
NaYF <sub>4</sub>	Yb, Er	SiO <sub>2</sub> - carcinoembryonic antigen (CEA)	HeLa HOS	N/A 92.6%	[124]
NaYF <sub>4</sub>	Yb, Er	SiO <sub>2</sub>	BMS cells	91.10%	[125]
NaYF <sub>4</sub>	Yb, Er	SiO <sub>2</sub>	skeletal myoblast	93.30%	[126]
NaYF <sub>4</sub>	Yb, Er	CaF <sub>2</sub> shells	HeLa	>90%	[127]
NaYF <sub>4</sub>	Yb, Er	Ab-siRNA3	SK-BR-3 cells	98.60% 92.50%	[128]
NaYF <sub>4</sub>	Yb, Er	SiO <sub>2</sub>	human osteosarcoma	96.20%	[107]
NaYF <sub>4</sub>	Yb, Er	No functionalization	HeLa	Not reported	[128]
LaF <sub>3</sub>	Yb, Ho	mPEG5	KB cells 4	>85%	[129]
NaYF <sub>4</sub>	Yb, Tm	PAA	KB cells	>94%	[103]
Y <sub>2</sub> O <sub>3</sub>	Yb, Er	SiO <sub>2</sub> -FA	HeLa, MCF7	>90	[130]
NaYF <sub>4</sub>	Yb, Er	HS-PEG HS-DNA	HeLa	Not reported	[131]
NaYF <sub>4</sub>	Yb, Er	AMPA, APTES, DHCA with POEGA-b-PMAEP (MAEP)	CHO-K1 cells	>95%	[132]

**Table 5.**  
*Surface modification and cell viability of UCNP reported by several authors.*

- **Confocal microscopy:** Confocal microscopy is a high-resolution imaging technique that allows for the visualization of NPs within cells. By using fluorescent labels or intrinsic luminescence properties of the NPs, confocal microscopy provides spatial information about the distribution and localization of NPs in cellular compartments.
- **Epifluorescence microscopy:** Epifluorescence microscopy is another imaging technique that utilizes fluorescence to visualize NPs within cells. It provides a wider field of view compared to confocal microscopy but with lower spatial resolution. It can be useful for qualitative assessments of NPs uptake and distribution.
- **Fluorometric quantification:** This technique involves measuring the fluorescence intensity of NPs, either in cell lysates or supernatants, using a fluorescence plate reader or spectrofluorometer. It allows for the quantitative determination of NPs uptake by cells and can be used to assess the cellular internalization over time.
- **Laser scanning microscopy:** Laser scanning microscopy, such as laser scanning confocal microscopy or multiphoton microscopy, provides high-resolution imaging capabilities to visualize NPs within cells. It offers the advantage of optical sectioning and 3D imaging, enabling detailed analysis of NPs distribution in different cellular compartments.

The selection of the appropriate technique depends on the specific characteristics of the NPs, the cellular system being studied, and the research objectives. Researchers may choose one or a combination of these techniques to gain a comprehensive understanding of the cellular uptake of NPs and their localization within cells [133].

The laser scanning microscope is a traditional fluorescence technique with the use of fluorescent biomarkers and dyes, but this method lacks the axial (z-axis) resolution to precisely detect the locations of intracellular NPs [134]. This limitation is overcome by employing confocal microscopy, which lends itself to two methods, namely confocal laser scanning microscopy and spinning disk confocal laser microscopy (CLSM). CLSM is widely used in biological research for high-resolution imaging. It employs point illumination and a pinhole aperture to eliminate out-of-focus light, resulting in improved axial resolution. The sample is scanned sequentially by a laser beam, and the emitted fluorescence light is collected through the same objective lens. By using a pinhole to block out-of-focus light, only the in-focus fluorescence from the focal plane is detected, providing sharper images and better localization of NPs within the cell.

Spinning disk confocal microscopy (SDCM) is another variant of confocal microscopy that utilizes a spinning disk with multiple apertures instead of a pinhole. The spinning disk contains an array of microlenses and pinholes, which allows simultaneous illumination and detection of multiple points in the sample. This enables faster image acquisition and is particularly advantageous for capturing rapid cellular processes or live cell imaging. Both CLSM and SDCM provide improved z-axis resolution compared to traditional fluorescence microscopy, enabling the precise detection and localization of intracellular NPs. Researchers can choose between these methods based on their specific experimental requirements, such as imaging speed, sample type, and the need for live cell imaging [135].

The advantages of using UCNPs are the narrow emission spectrum, high expression, and long-term observation in comparison with the dye molecules that presented photo-bleaching, and they are not suitable for long-term observation by using fluorophores. Chatterjee and collaborators [121] reported the first use of NaYF<sub>4</sub>: Yb, Er UCNPs for cellular imaging functionalized with PEI and conjugated with FA. They worked with human HT29 adenocarcinoma cells and human OVCAR3 ovarian carcinoma cells and confirmed the internalization of the UCNP into both types of cells, the UCNPs emitted in green under a confocal microscope equipped with a 980 nm laser.

Confocal microscopy is an essential imaging technique for visualizing and analyzing the labeled cancer cells, allowing for high-resolution imaging and precise localization of the UCNPs within the cells. It provides researchers with valuable information about the cellular distribution and interaction of UCNPs with specific targets, aiding in the understanding of cancer biology and facilitating the development of targeted therapies.

The study conducted by Chao Wang and collaborators in 2011 [124] focused on the functionalization of UCNPs with polyethylene glycol (PEG) and the subsequent loading of the anticancer drug doxorubicin (DOX) onto the UCNPs. The loading of DOX onto the UCNPs was achieved through simple physical adsorption using a supramolecular chemistry approach. One of the key aspects of this study was the control of DOX loading and release from the UCNPs, which was achieved by manipulating the pH conditions. They observed that the dissociation rate of DOX from the UCNPs increased in an acidic environment, which is favorable for controlled drug release within the intracellular environment. The intracellular delivery of DOX by the functionalized UCNPs was demonstrated through imaging using a confocal

microscope. This technique allowed the researchers to visualize and confirm the successful delivery of the drug to the targeted cells. This study highlights the potential of functionalized UCNPs as drug carriers for intracellular drug delivery.

The ability to control drug release in response to specific conditions, such as pH, offers opportunities for targeted and controlled drug delivery systems with reduced side effects. The use of confocal microscopy for imaging provides valuable insights into the cellular uptake and intracellular distribution of the drug-loaded UCNPs [5].

For *in vivo* applications several authors reported internalization and visualization of UCNPs with different techniques. The limit for cell detection via UCNPs imaging is a relevant parameter to determine the sensitivity of the *in vivo* imaging technique by UCNPs. Liu and coworkers [120] proved that the 800 nm emissions from UCNPs consisting of sub-10 nm hexagonal NaLuF<sub>4</sub>: Yb can penetrate through a whole black mouse with a depth of ~2 cm, under excitation with a 980 nm laser using a confocal microscope. Also, they reported the study of lymphatic drainage in various parts of the body, for the diagnosis and treatment of cancer. They developed a UCNPs of LaF<sub>3</sub>: Yb, Tm and applied it for lymphatic system imaging *in vivo* with a high signal-to-noise ratio (~33) of the UCNPs signal (em = 800 nm). An intense UCNPs signal was observed from the removed lymph node, whereas no obvious UCNPs signal was detected from the area outside of the draining lymphatic system.

Epifluorescence microscopy is a useful technique for imaging thick samples, particularly those that are over 10 μm deep. However, it has some limitations, such as the potential for high background signal due to intense illumination and excitation of molecules outside the focal plane. Despite this, several authors have successfully utilized epifluorescence microscopy for bioimaging with UCNPs.

One study by Mrazek and colleagues [107] introduced a modification to the epifluorescence microscope that enabled quantitative widefield imaging of UCNPs. They incorporated a tandem microlens array, a moving diffuser, and a telescope into their setup. By adjusting the top-hat area to the field of view, they achieved a high level of illumination profile homogeneity, reaching approximately 98%. This modified illuminator was combined with the epifluorescence attachment of the microscope, allowing for easy switching between observation of UCNPs and traditional fluorescent dyes.

In another study by Yang and colleagues [129], a quantitative fluorescence image analysis based on multicolor UCNPs was developed for the detection of ochratoxin A and zearalenone. They first obtained a clear image of the UCNPs using near-infrared (NIR) excitation. Then, with the appropriate filters and detection methods, they were able to detect the presence of the target analytes using the fluorescence signals emitted by the UCNPs. These studies demonstrate the successful utilization of epifluorescence microscopy for imaging UCNPs and their applications in quantitative analysis. The modifications made to the microscopy setup and the careful selection of excitation and detection parameters contribute to enhancing the sensitivity and accuracy of the imaging process.

Flow cytometry is indeed a powerful technique for the analysis of cellular internalization of fluorescently labeled NPs. It allows for the quantitative measurement of the proportion of cells that have taken up the labeled NPs. Flow cytometry utilizes laser-based excitation and detection of fluorescence signals emitted by the labeled NPs, providing a high statistical analysis of a large number of cells. One of the main advantages of flow cytometry is its ability to analyze a large population of cells rapidly, providing statistical data on the percentage of cells that have internalized the NPs. It can also provide information on the level of NP uptake within individual cells by measuring the fluorescence intensity.

However, it is important to note that flow cytometry has its limitations. One of the main drawbacks is its relatively low resolution, which makes it challenging to study the precise localization of NPs within different cellular compartments. Flow cytometry primarily provides information on whether the NPs have been internalized by the cells, but it cannot determine their specific subcellular localization or membrane-bound interactions. Therefore, while flow cytometry is an excellent method for the detection and quantification of cellular internalization of NPs, it is often complemented by other techniques such as fluorescence microscopy or electron microscopy to gain more detailed information about NP localization within cells and their interactions with cellular structures.

Juarez-Moreno et al. analyzed the internalization of UCNPs functionalized with FA in B16-F10 melanoma cancer cells, and for negative control they used the L929 cell line because it does not have folic acid receptors on the membrane. The uptake of FA-UCNPs into cells was determined in terms of cell granularity, also known as intracellular complexity, which was detected by the side scatter beam (SSC-H) of the flow cytometer. They compared the internalization of the UCNPs into 2D and 3D cell arrays and concluded that the internalization of the nanoparticles was concentration dependent. The internalization of FA-UCNPs was higher in melanoma B16-F10 cells in a 3D conformation than in 2D cultures [130].

Indeed, the unique properties of UCNPs make them highly attractive for bioimaging applications. UCNPs offer several advantages over conventional biomarkers and therapeutic agents, making them promising candidates for various biomedical applications. However, further research is still needed to fully understand the behavior of UCNPs in complex biological systems, especially in live animals. This includes studying their biodistribution, pharmacokinetics, long-term toxicity, and clearance mechanisms. Comprehensive nanotoxicological assessments are crucial to ensure the safe use of UCNPs in biomedical applications.

By gaining a deeper understanding of the behavior and potential risks associated with UCNPs, researchers can develop strategies to optimize their properties, improve their biocompatibility, and minimize any potential adverse effects. This knowledge will contribute to the development of safe and effective UCNPs for various biomedicine applications, including bioimaging, drug delivery, and theranostic.

Overall, UCNPs hold great promise in the field of biomedicine, but continued research and evaluation are necessary to unlock their full potential and ensure their safe and efficient use in clinical settings.

## 5. Conclusions

In summary, upconversion nanoparticles (UCNPs) exhibit great promise in the realms of bioimaging and theranostic applications, thanks to their efficient near-infrared-triggered emissions, large anti-Stokes shifts, high sensitivity, and biocompatibility. Despite their potential, several challenges necessitate attention for optimal utilization:

1. **Emission Properties:** The surface properties of UCNPs can impact emission ratios, leading to monochromatic emissions. Addressing this involves refining the synthesis process by selecting appropriate host lattices and activators.
2. **Quantum Yield and Deep Tissue Imaging:** Low quantum yields of  $\text{Ln}^{3+}$  ions limit UCNPs' applications for deep tissue imaging. Strategies involve enhancing

upconversion efficiency through doping UCNPs and exploring alternative activators like  $\text{Yb}^{3+}$ .

3. Expansion to Other Biological Models: While promising *in vitro* and small animal studies, UCNPs' application in diverse biological models, such as plants or large animals, is limited and requires further testing.
4. Tumor Targeting and Intravenous Injection: Improving targeting capabilities to specific tumor tissues and enabling intravenous injection would enhance precision in cancer therapy.
5. Drug Delivery and Therapeutics: Optimizing UCNPs as carriers for therapeutic molecules requires focusing on controlled release, stimuli-responsive behavior, and multi-functional payloads for targeted therapies.
6. Imaging and Sensing Modalities: Integrating UCNPs with various bioimaging techniques and sensing platforms could improve diagnostic capabilities and open new avenues for biosensing.
7. Scalability and Cost-effectiveness: Streamlining synthesis methods for scalable and cost-effective manufacturing is crucial for widespread adoption.
8. Multifunctional Platforms: Exploring integration with other nanomaterials or technologies could lead to the development of multifunctional platforms with enhanced properties.
9. Overheating Issue: Exploring alternative excitation wavelengths, such as 880 nm NIR, and optimizing activator choices, especially  $\text{Yb}^{3+}$ , can mitigate the overheating issue associated with the typical 980 nm laser.
10. Nanotoxicological Assessment: Further analysis and a comprehensive approach considering LNPs architecture, cell biology, and predictive computer-aided tools are necessary for a deeper understanding of nanotoxicity.

Overall, the field of UCNPs for bioimaging and chemotherapeutic delivery holds enormous potential. By addressing the challenges mentioned and conducting further research, the development of next-generation nano-engineered LNPs with enhanced properties and translational potential for clinical applications is within reach.

## Acknowledgements

The authors wish to acknowledge the support of CETYS University and Universidad Latina de Panama.

## Conflicts of interest

The authors declare no conflict of interest.

IntechOpen

## Author details

Dalia Chávez-García<sup>1\*</sup> and Mario Guzman<sup>2</sup>


1 Universidad Latina de Panama, Panama

2 Centro de Enseñanza Técnica y Superior (CETYS), Ensenada, México

\*Address all correspondence to: [daliachavez@ulatina.edu.pa](mailto:daliachavez@ulatina.edu.pa)

## IntechOpen

---

© 2024 The Author(s). Licensee IntechOpen. This chapter is distributed under the terms of the Creative Commons Attribution License (<http://creativecommons.org/licenses/by/3.0>), which permits unrestricted use, distribution, and reproduction in any medium, provided the original work is properly cited. 



## References

- [1] Rihn BH. Biomedical Application of Nanoparticles. 1st ed. Boca Raton, FL: Taylor & Francis Group L, CRC Press; 2018. 321 p
- [2] Zhong Y, Dai H. A mini-review on rare-earth down-conversion nanoparticles for NIR-II imaging of biological systems. In: Nano Research. Vol. 13, no. 5. Beijing, China: Tsinghua University Press; 2020. pp. 1281-1294. DOI: 10.1007/s12274-020-2721-0
- [3] Wan J, Wang Z, Chen X, Mu L, Qian Y. Shape-tailored photoluminescent intensity of red phosphor  $Y_2O_3:Eu^{3+}$ . Journal of Crystal Growth. 2005;284:538-543
- [4] Wang W, Sun Z, He X, Wei Y, Zou Z, Zhang J. How to design ultraviolet emitting persistent materials for potential multifunctional applications: A living example of a  $NaLuGeO_4:Bi^{3+}, Eu^{3+}$  phosphor. Journal of Materials Chemistry C Materials. 2017;5(17):4310-4318. DOI: 10.1039/C6TC05598B
- [5] Wang M, Abbineni G, Clevenger A, Mao C, Xu S. Upconversion nanoparticles: Synthesis, surface modification and biological applications. Nanomedicine: Nanotechnology, Biology, and Medicine. 2011;7(6):710-729. DOI: 10.1016/j.nano.2011.02.013
- [6] Blasse G, Grabmaier BC. Luminescent Materials. Berlin Heidelberg: Springer-Verlag; 1994. p. 230. DOI: 10.1021/ja965667t
- [7] Blasse G, Grabmaier BC. A general introduction to luminescent materials. In: Luminescent Materials. Berlin, Heidelberg: Springer; 2011. DOI: 10.1007/978-3-642-79017-1\_1
- [8] Blasse G, Grabmaier BC. How does a luminescent material absorb its excitation energy? In: Luminescent Materials. Berlin, Heidelberg: Springer Science & Business Media; 2011. DOI: 10.1007/978-3-642-79017-1\_2
- [9] Vetrone F, Boyer JC, Capobianco JA, Speghini A, Bettinelli M. Significance of  $Yb^{3+}$  concentration on the upconversion mechanisms in codoped  $Y_2O_3:Er^{3+}, Yb^{3+}$  nanocrystals. Journal of Applied Physics. 2004;96(1):661-667. DOI: 10.1063/1.1739523
- [10] Chavez D, Contreras HG. Synthesis and upconversion luminescence of nanoparticles  $Y_2O_3$  and  $Gd_2O_3$  Co-doped with  $Yb^{3+}$  and  $Er^{3+}$ . Nanomaterials and Nanotechnology. 2016;6:7. DOI: 10.5772/62188
- [11] Lojpur V, Nikolic M, Mancic L, Milosevic O, Dramicanin MD.  $Y_2O_3:Yb, Tm$  and  $Y_2O_3:Yb, Ho$  powders for low-temperature thermometry based on up-conversion fluorescence. Ceramics International. 2013;39(2):1129-1134
- [12] Su J, Song F, Tan H, Han L, Zhou F, Tian J. Phonon-assisted mechanisms and concentration dependence of  $Tm^{3+}$  blue upconversion luminescence in codoped  $NaY(WO_4)_2$  crystals. Journal of Physics D: Applied Physics. 2006;39(10):2094-2099. DOI: 10.1088/0022-3727/39/10/019
- [13] Šević D, Rabasović MS, Križan J, Savić-Šević S, Rabasović MD, Marinkovic BP. Effects of temperature on luminescent properties of  $Gd_2O_3:Er, Yb$  nanophosphor. Optical and Quantum Electronics. 2020;52(5):232. DOI: 10.1007/s11082-020-02348-y
- [14] Yang J, Zhang C, Peng C, Li C, Wang L, Chai R. Controllable red, green, blue (RGB) and bright white upconversion luminescence of

Lu<sub>2</sub>O<sub>3</sub>: Yb<sup>3+</sup>/Er<sup>3+</sup>/Tm<sup>3+</sup> nanocrystals through single laser excitation at 980 nm. *Chemistry – A European Journal* [Internet]. 2009;**15**(18):4649-4655. DOI: 10.1002/chem.200802106

[15] Han Q, Yan T, Song Y, Wang Y, Zhang X. Up-conversion luminescence enhancement and tunable emission color of Y<sub>2</sub>O<sub>3</sub>: Tm/Yb@Y<sub>2</sub>O<sub>3</sub>: Yb@Y<sub>2</sub>O<sub>3</sub>: Er/Yb multilayer thin films. *Journal of Alloys and Compounds*. 2021;**877**:160151. DOI: 10.1016/j.jallcom.2021.160151

[16] Das GK, Tan TTY. Rare-earth-doped and codoped Y<sub>2</sub>O<sub>3</sub> nanomaterials as potential bioimaging probes. *Journal of Physical Chemistry C*. 2008;**112**(30):11211-11217. DOI: 10.1021/jp802076n

[17] Chávez-García D, Juárez-Moreno K, Hirata GA. Upconversion nanoparticles Y<sub>2</sub>O<sub>3</sub> and Gd<sub>2</sub>O<sub>3</sub> Co-doped with Er<sup>3+</sup> and Yb<sup>3+</sup> with aminosilane-folic acid functionalization for breast and cervix cancer cells detection. *MRS Advances*. 2017;**2**(52):2983-2988. DOI: 10.1557/adv.2017.447

[18] Hemmer E, Venkatachalam N, Hyodo H, Hattori A, Ebina Y, Kishimoto H. Upconverting and NIR emitting rare earth based nanostructures for NIR-bioimaging. *Nanoscale*. 2013;**5**(23):11339-11361. DOI: 10.1039/C3NR02286B

[19] Liu C, Chen D. Controlled synthesis of hexagon shaped lanthanide-doped LaF<sub>3</sub> nanoplates with multicolor upconversion fluorescence. *Journal of Materials Chemistry*. 2007;**17**(37):3875-3880. DOI: 10.1039/B707927C

[20] Pires AM, Serra OA, Davolos MR. Yttrium oxysulfide nanosized spherical particles doped with Yb and Er or Yb and Tm: Efficient materials for up-converting phosphor technology field. *Journal of*

*Alloys and Compounds*. 2004;**374**:181-184. DOI: 10.1016/j.jallcom.2003.11.088

[21] Steblevskaya NI, Medkov MA, Belobeletskaya MV. Luminophores and protective coatings based on oxides and oxysulfides of rare-earth elements prepared by extraction pyrolysis. *Theoretical Foundations of Chemical Engineering*. 2014;**48**(4):449-453. DOI: 10.1134/S0040579514040125

[22] De HP, Huang XG, Zhang QT. Effect of doping concentration on the up-conversion luminescent properties of Y<sub>2</sub>O<sub>3</sub>:Yb, Tm phosphors. *Advanced Materials Research*. 2011;**197-198**:558-562. DOI: 10.4028/www.scientific.net/AMR.197-198.558

[23] Hirai T, Orikoshi T. Preparation of Gd<sub>2</sub>O<sub>3</sub>: Yb, Er and Gd<sub>2</sub>O<sub>2</sub>S: Yb, Er infrared-to-visible conversion phosphor ultrafine particles using an emulsion liquid membrane system. *Journal of Colloid and Interface Science*. 2004;**269**(1):103-108. DOI: 10.1016/j.jcis.2003.08.026

[24] Kataria V, Mehta DS. Investigation of concurrent emissions in visible, UV and NIR region in Gd<sub>2</sub>O<sub>2</sub>S: Er, Yb nanophosphor by diverse excitation wavelengths as a function of firing temperature. *Optical Materials (Amst)*. 2019;**95**:109204. DOI: 10.1016/j.optmat.2019.109204

[25] Du YP, Zhang YW, Sun LD, Yan CH. Luminescent monodisperse nanocrystals of lanthanide oxyfluorides synthesized from trifluoroacetate precursors in high-boiling solvents. *The Journal of Physical Chemistry C*. 2008;**112**(2):405-415. DOI: 10.1021/jp076717r

[26] Gao D, Gao F, Wu J, Kuang Q, Xing C, Chen W. Up-conversion luminescence performance and application of GdOF: Yb, Er porous spheres obtained by calcining NaGdF<sub>4</sub>:

- Yb, Er microcrystals. *Applied Surface Science*. 2022;**587**:152820. DOI: 10.1016/j.apsusc.2022.152820
- [27] Gao L, Ge X, Chai Z, Xu G, Wang X, Wang C. Shape-controlled synthesis of octahedral  $\alpha$ - $\text{NaYF}_4$  and its rare earth doped submicrometer particles in acetic acid. *Nano Research*. 2009;**2**(7):565-574. DOI: 10.1007/s12274-009-9056-1
- [28] Kang M, Kang HB, Park S, Jang HS. Facile synthesis of sub-10 nm-sized bright red-emitting upconversion nanophosphors via tetrahedral YOF: Yb, Er seed-mediated growth. *Chemical Communications*. 2019;**55**(89):13350-13353. DOI: 10.1039/C9CC06797C
- [29] AitMellal O, Oufni L, Messous MY, Trandafir MM, Chirica IM, Florea M. Comparative investigation of structural, EPR, optical and photoluminescence properties of nanostructured  $\text{LaPO}_4$ : Ce/RE/me and  $\text{LaPO}_4$ : Yb/Er phosphors prepared by co-precipitation method. *Journal of Solid State Chemistry*. 2021;**301**:122310. DOI: 10.1016/j.jssc.2021.122310
- [30] Lisiecki R, Ryba-Romanowski W, Speghini A, Bettinelli M. Luminescence spectroscopy of  $\text{Er}^{3+}$ -doped and  $\text{Er}^{3+}$ ,  $\text{Yb}^{3+}$ -codoped  $\text{LaPO}_4$  single crystals. *Journal of Luminescence*. 2009;**129**(5):521-525. DOI: 10.1016/j.jlumin.2008.12.006
- [31] Heer S, Lehmann O, Haase M, Güdel HU. Blue, green, and red upconversion emission from lanthanide-doped  $\text{LuPO}_4$  and  $\text{YbPO}_4$  nanocrystals in a transparent colloidal solution. *Angewandte Chemie International Edition*. 2003;**42**(27):3179-3182. DOI: 10.1002/anie.200351091
- [32] Yi G, Sun B, Yang F, Chen D, Zhou Y, Cheng J. Synthesis and characterization of high-efficiency nanocrystal up-conversion phosphors: Ytterbium and erbium codoped lanthanum molybdate. *Chemistry of Materials*. 2002;**14**(7):2910-2914. DOI: 10.1021/cm0115416
- [33] Chen Z, Bu W, Zhang N, Shi J. Controlled construction of monodisperse  $\text{La}_2(\text{MoO}_4)_3$ : Yb, Tm microarchitectures with upconversion luminescent property. *The Journal of Physical Chemistry C*. 2008;**112**(11):4378-4383. DOI: 10.1021/jp711213r
- [34] Zhou Y, He XH, Yan B. Self-assembled  $\text{RE}_2(\text{MO}_4)_3$ :  $\text{Ln}^{3+}$  (RE=Y, La, Gd, Lu; M=W, Mo; Ln=Yb/Er, Yb/Tm) hierarchical microcrystals: Hydrothermal synthesis and up-conversion luminescence. *Optical Materials (Amst)*. 2014;**36**(3):602-607. DOI: 10.1016/j.optmat.2013.10.036
- [35] Yu W, Tian Y, Xing M, Fu Y, Zhang H, Luo X. Up-conversion luminescence of  $\text{NaY}(\text{WO}_4)_2$ : Yb, Er under 1550 and 980 nm excitation. *Materials Research Bulletin*. 2016;**80**:223-229. DOI: 10.1016/j.materresbull.2016.03.013
- [36] Xue N, Fan X, Wang Z, Wang M. Synthesis process and luminescence properties of  $\text{Ln}^{3+}$  doped  $\text{NaY}(\text{WO}_4)_2$  nanoparticles. *Materials Letters*. 2007;**61**(7):1576-1579. DOI: 10.1016/j.matlet.2006.07.082
- [37] Sun C, Lü W, Yang F, Tu C. Tunable red-green-blue multicolor luminescence in  $\text{Yb}^{3+}/\text{Tm}^{3+}/\text{Ho}^{3+}$ :  $\text{Gd}_3\text{Ga}_5\text{O}_{12}$  nano-crystals. *Journal of Alloys and Compounds*. 2012;**512**(1):160-164. DOI: 10.1016/j.jallcom.2011.09.056
- [38] Pandozzi F, Vetrone F, Boyer JC, Naccache R, Capobianco JA, Speghini A. A spectroscopic analysis of blue and ultraviolet upconverted emissions from  $\text{Gd}_3\text{Ga}_5\text{O}_{12}$ :  $\text{Tm}^{3+}$ ,  $\text{Yb}^{3+}$  nanocrystals. *Journal of Physical Chemistry B*. 2005;**109**(37):17400-17405. DOI: 10.1021/jp052192w

- [39] Tsuboi T. Upconversion emission in  $\text{Er}^{3+}/\text{Yb}^{3+}$ -codoped  $\text{YVO}_4$  crystals. *Physical Review B*. 2020;**62**(7):4200. DOI: 10.1103/PhysRevB.62.4200
- [40] Ma R, Shimmon R, McDonagh A, Maynard P, Lennard C, Roux C. Fingerprint detection on non-porous and semi-porous surfaces using  $\text{YVO}_4$ : Er, Yb luminescent upconverting particles. *Forensic Science International*. 2012;**217**(1):e23-e26. DOI: 10.1016/j.forsciint.2011.10.033
- [41] Wang K, Ma J, He M, Gao G, Xu H, Sang J, et al. Toxicity assessments of near-infrared upconversion luminescent  $\text{LaF}_3$ : Yb, Er in early development of zebrafish embryos. *Theranostics*. 2013;**3**(4):258-266. DOI: 10.7150/thno.5701
- [42] Yi GS, Chow GM. Colloidal  $\text{LaF}_3$ : Yb, Er,  $\text{LaF}_3$ : Yb, Ho and  $\text{LaF}_3$ : Yb, Tm nanocrystals with multicolor upconversion fluorescence. *Journal of Materials Chemistry*. 2005;**15**(41):4460-4464. DOI: 10.1039/B508240D
- [43] Huang X. Enhancement of near-infrared to near-infrared upconversion luminescence in sub-10-nm ultra-small  $\text{LaF}_3$ : $\text{Yb}^{3+}$ / $\text{Er}^{3+}$ / $\text{Tm}^{3+}$  nanoparticles through lanthanide doping. *Optics Letters*. 2015;**40**(22):5231-5234. Available from: <https://opg.optica.org/ol/abstract.cfm?URI=ol-40-22-5231>
- [44] Wang X, Hu Z, Sun M, Du P, Liu W, Huang S, et al. Phase-conversion synthesis of  $\text{LaF}_3$ : Yb/RE (RE = Ho, Er) nanocrystals with  $\text{Ln}_2(\text{OH})_4\text{SO}_4 \cdot 2\text{H}_2\text{O}$  type layered compound as a new template, phase/morphology evolution, and upconversion luminescence. *Journal of Materials Research and Technology*. 2020;**9**(5):10659-10668. Available from: <https://www.sciencedirect.com/science/article/pii/S2238785420315684>
- [45] Hu H, Chen Z, Cao T, Zhang Q, Yu M, Li F, et al. Hydrothermal synthesis of hexagonal lanthanide-doped  $\text{LaF}_3$  nanoplates with bright upconversion luminescence. *Nanotechnology*. 2008;**19**(37):375702. DOI: 10.1088/0957-4484/19/37/375702
- [46] Xie J, Hu W, Tian D, Wei Y, Zheng G, Huang L, et al. Selective growth and upconversion photoluminescence of Y-based fluorides: From  $\text{NaYF}_4$ : Yb/Er to  $\text{YF}_3$ : Yb/Er crystals. *Nanotechnology* [Internet]. 2020;**31**(50):505605. DOI: 10.1088/1361-6528/abb627
- [47] Suo H, Hu F, Zhao X, Zhang Z, Li T, Duan C, et al. All-in-one thermometer-heater up-converting platform  $\text{YF}_3$ :  $\text{Yb}^{3+}$ ,  $\text{Tm}^{3+}$  operating in the first biological window. *Journal of Materials Chemistry C Materials* [Internet]. 2017;**5**(6):1501-1507. DOI: 10.1039/C6TC05449H
- [48] Yan RX, Li YD. Down/up conversion in  $\text{Ln}^{3+}$ -doped  $\text{YF}_3$  nanocrystals. *Advanced Functional Materials* [Internet]. 2005;**15**(5):763-770. DOI: 10.1002/adfm.200305044
- [49] Bartkowiak A, Siejca A, Borkowski K, Lis S, Grzyb T. Up-converting  $\text{LuF}_3$  and  $\text{NaLuF}_4$  fluorides doped with  $\text{Yb}^{3+}/\text{Er}^{3+}$  or  $\text{Yb}^{3+}/\text{Tm}^{3+}$  ions for latent fingerprints detection. *Journal of Alloys and Compounds*. 2019;**784**:641-652. DOI: 10.1016/j.jallcom.2018.12.344
- [50] Wang G, Qin W, Zhang J, Zhang J, Wangyan CC, et al. Synthesis, growth mechanism, and tunable upconversion luminescence of  $\text{Yb}^{3+}/\text{Tm}^{3+}$ -codoped  $\text{YF}_3$  nanobundles. *The Journal of Physical Chemistry C* [Internet]. 2008;**112**(32):12161-12167. DOI: 10.1021/jp8004713
- [51] Homann C, Krukewitt L, Frenzel F, Grauel B, Würth C, Resch-Genger U, et al.  $\text{NaYF}_4$ : Yb,Er/ $\text{NaYF}_4$  core/shell nanocrystals with high upconversion luminescence quantum yield.

Angewandte Chemie International Edition. 2018;**57**(28):8765-8769. DOI: 10.1002/anie.201803083

[52] Yuan Z, Lin C, Wang Y, Niu Y, Yan J, Lu M, et al. Anion additive-induced size, morphology, and local structure tuning of lanthanide-doped upconversion nanoparticles. *Advanced Materials Interfaces* [Internet]. 2022;**9**:2201277. DOI: 10.1002/admi.202201277

[53] Wang M, Liu JL, Zhang YX, Hou W, Wu XL, Xu SK. Two-phase solvothermal synthesis of rare-earth doped NaYF<sub>4</sub> upconversion fluorescent nanocrystals. *Materials Letters*. 2009;**63**(2):325-327. DOI: 10.1016/j.matlet.2008.10.028

[54] Tang Y, Di W, Zhai X, Yang R, Qin W. NIR-responsive photocatalytic activity and mechanism of NaYF<sub>4</sub>: Yb, Tm@TiO<sub>2</sub> Core-Shell nanoparticles. *ACS Catalysis* [Internet]. 2013;**3**(3):405-412. DOI: 10.1021/cs300808r

[55] Lingeshwar Reddy K, Srinivas V, Shankar KR, Kumar S, Sharma V, Kumar A, et al. Enhancement of luminescence intensity in red emitting NaYF<sub>4</sub>: Yb/Ho/Mn upconversion nanophosphors by variation of reaction parameters. *The Journal of Physical Chemistry C* [Internet]. 2017;**121**(21):11783-11793. DOI: 10.1021/acs.jpcc.7b01334

[56] Hong AR, Kim SY, Cho SH, Lee K, Jang HS. Facile synthesis of multicolor tunable ultrasmall LiYF<sub>4</sub>: Yb, Tm, Er/LiGdF<sub>4</sub> core/shell upconversion nanophosphors with sub-10 nm size. *Dyes and Pigments*. 2017;**139**:831-838. DOI: 10.1016/j.dyepig.2016.12.048

[57] Naccache R, Vetrone F, Mahalingam V, Cuccia LA, Capobianco JA. Controlled synthesis and water dispersibility of hexagonal

phase NaGdF<sub>4</sub>: Ho<sup>3+</sup>/Yb<sup>3+</sup> nanoparticles. *Chemistry of Materials* [Internet]. 2009;**21**(4):717-723. DOI: 10.1021/cm803151y

[58] Liang L, Zhang X, Hu H, Feng L, Wu M, Su Q. Up-conversion properties in KGd<sub>2</sub>F<sub>7</sub>: Yb<sup>3+</sup>/Er<sup>3+</sup>. *Materials Letters*. 2005;**59**(17):2186-2190. DOI: 10.1016/j.matlet.2005.02.061

[59] Yu L, Li G, Liu Y, Jiang F, Hong M. Lanthanide-doped KGd<sub>2</sub>F<sub>7</sub> nanocrystals: Controlled synthesis, optical properties, and spectroscopic identification of the optimum core/shell architecture for highly enhanced upconverting luminescence. *Crystal Growth & Design*. 2019;**19**(4):2340-2349. DOI: 10.1021/acs.cgd.9b00040

[60] Niu N, Yang P, Liu Y, Li C, Wang D, Gai S, et al. Controllable synthesis and up-conversion properties of tetragonal BaYF<sub>5</sub>:Yb/In (In=Er, Tm, and Ho) nanocrystals. *Journal of Colloid and Interface Science*. 2011;**362**(2):389-396. DOI: 10.1016/j.jcis.2011.07.001

[61] Luo R, Chen L, Li Q, Zhou J, Mei L, Ning Z, et al. Bi<sup>3+</sup>-doped BaYF<sub>5</sub>:Yb,Er Upconversion nanoparticles with enhanced luminescence and application case for X-ray computed tomography imaging. *Inorganic Chemistry*. 2020;**59**(24):17906-17915. DOI: 10.1021/acs.inorgchem.0c01818

[62] Vetrone F, Mahalingam V, Capobianco JA. Near-infrared-to-blue upconversion in colloidal BaYF<sub>5</sub>: Tm<sup>3+</sup>, Yb<sup>3+</sup> nanocrystals. *Chemistry of Materials*. 2009;**21**(9):1847-1851. DOI: 10.1021/cm900313s

[63] Smet PF, Moreels I, Hens Z, Poelman D. Luminescence in sulfides: A rich history and a bright future. *Materials* [Internet]. 2010;**3**(4):2834-2883. DOI: 10.3390/ma3042834

- [64] Wu W, He Q, Jiang C. Magnetic iron oxide nanoparticles: Synthesis and surface functionalization strategies. *Nanoscale Research Letters*. 2008;**3**(11):397-415. DOI: 10.1007/s11671-008-9174-9
- [65] Priya R, Pandey OP, Dhoble SJ. Review on the synthesis, structural and photo-physical properties of Gd<sub>2</sub>O<sub>3</sub> phosphors for various luminescent applications. *Optics and Laser Technology*. 2021;**135**:106663. DOI: 10.1016/j.optlastec.2020.106663
- [66] Fang Z, Yu H, Zhang B, Jiang D, Wu Q, Xiong L, et al. Suppression of Eu<sup>2+</sup> luminescence and enhancement of Eu<sup>3+</sup> emission in Eu: CaF<sub>2</sub> single crystal via Gd<sup>3+</sup> co-doping. *Journal of Luminescence*. 2021;**233**:117877. DOI: 10.1016/j.jlumin.2020.117877
- [67] Werts MHV. Making sense of lanthanide luminescence. *Science Progress*. 2005;**88**(2):101-131. DOI: 10.3184/003685005783238435
- [68] Iqbal S, Fakhar-e-Alam M, Alimgeer KS, Atif M, Hanif A, Yaqub N, et al. Mathematical modeling and experimental analysis of the efficacy of photodynamic therapy in conjunction with photo thermal therapy and PEG-coated Au-doped TiO<sub>2</sub> nanostructures to target MCF-7 cancerous cells. *Saudi Journal of Biological Sciences*. 2021;**28**(2):1226-1232. DOI: 10.1016/j.sjbs.2020.11.086
- [69] Dos Santos CCL, Passos Farias IA, de Jesus dos Reis Albuquerque A, Silva DPMFE, da Costa One GM, Sampaio FC. Antimicrobial activity of nano cerium oxide (IV) (CeO<sub>2</sub>) against *Streptococcus mutans*. *BMC Proceedings*. 2014;**8**(4):P48. DOI: 10.1186/1753-6561-8-S4-P48
- [70] Barar J, Kafil V, Majd MH, Barzegari A, Khani S, Johari-Ahar M, et al. Multifunctional mitoxantrone-conjugated magnetic nanosystem for targeted therapy of folate receptor-overexpressing malignant cells. *Journal of Nanobiotechnology*. 2015;**13**(1):26. DOI: 10.1186/s12951-015-0083-7
- [71] Park J, Joo J, Kwon SG, Jang Y, Hyeon T. Synthesis of monodisperse spherical nanocrystals. *Angewandte Chemie International Edition*. 2007;**46**(25):4630-4660. DOI: 10.1002/anie.200603148
- [72] Taxak VB, Khatkar SP, Do HS, Kumar R, Kumar M. Tartaric acid-assisted sol – gel synthesis of Y<sub>2</sub>O<sub>3</sub>: Eu<sup>3+</sup> nanoparticles. *Journal of Alloys and Compounds*. 2009;**469**:224-228. DOI: 10.1016/j.jallcom.2008.01.088
- [73] Talane TE, Mbule PS, Noto LL, Shingange K, Mhlongo GH, Mothudi BM, et al. Sol-gel preparation and characterization of Er<sup>3+</sup> doped TiO<sub>2</sub> luminescent nanoparticles. *Materials Research Bulletin*. 2018;**108**:234-241. DOI: 10.1016/j.materresbull.2018.09.007
- [74] Ai X, Aw J, Xing B. Upconversion nanoparticles for bioimaging. In: Liu RS, editor. *Phosphors, Up Conversion Nano Particles, Quantum Dots and their Applications*. Vol. 2. Singapore: Springer Singapore; 2016. pp. 363-390. DOI: 10.1007/978-981-10-1590-8\_12
- [75] Boyer JC, Vetrone F, Cuccia LA, Capobianco JA. Synthesis of colloidal upconverting NaYF<sub>4</sub> nanocrystals doped with Er<sup>3+</sup>, Yb<sup>3+</sup> and Tm<sup>3+</sup>, Yb<sup>3+</sup> via thermal decomposition of lanthanide trifluoroacetate precursors. *Journal of the American Chemical Society*. 2006;**128**(23):7444-7445. DOI: 10.1021/ja061848b
- [76] Li C, Yang J, Quan Z, Yang P, Kong D, Lin J. Different microstructures of β-NaYF<sub>4</sub> fabricated by hydrothermal

process: Effects of pH values and fluoride sources. *Chemistry of Materials*. 2007;**19**(20):4933-4942. DOI: 10.1021/cm071668g

[77] Yi G, Lu H, Zhao S, Ge Y, Yang W, Chen D, et al. Synthesis, characterization, and biological application of size-controlled nanocrystalline NaYF<sub>4</sub>: Yb, Er infrared-to-visible up-conversion phosphors. *Nano Lett*. 2004;**4**(11):2191-2196. DOI: 10.1021/nl048680h

[78] Pandey A, Rai VK, Dey R, Kumar K. Enriched green upconversion emission in combustion synthesized Y<sub>2</sub>O<sub>3</sub>: Ho<sup>3+</sup>-Yb<sup>3+</sup> phosphor. *Materials Chemistry and Physics*. 2013;**139**(2):483-488. Available from: <https://www.sciencedirect.com/science/article/pii/S0254058413000874>

[79] Li Y, Chen R, Li Y, Sharafudeen K, Liu S, Wu D, et al. Folic acid-conjugated chromium(III) doped nanoparticles consisting of mixed oxides of zinc, gallium and tin, and possessing near-infrared and long persistent phosphorescence for targeted imaging of cancer cells. *Microchimica Acta*. 2015;**182**(9-10):1827-1834. DOI: 10.1007/s00604-015-1486-8

[80] Sudimack J, Lee RJ. Targeted drug delivery via the folate receptor. *Advanced Drug Delivery Reviews*. 2000;**41**(2):147-162. DOI: 10.1016/S0169-409X(99)00062-9

[81] Chakraborti S, Chakraborty S, Saha S, Manna A, Banerjee S, Adhikary A, et al. PEG-functionalized zinc oxide nanoparticles induce apoptosis in breast cancer cells through reactive oxygen species-dependent impairment of DNA damage repair enzyme NEIL2. *Free Radical Biology & Medicine*. 2017;**103**:35-47. DOI: 10.1016/j.freeradbiomed.2016.11.048

[82] Cheng J, Teply BA, Sherifi I, Sung J, Luther G, Gu FX, et al. Formulation of

functionalized PLGA-PEG nanoparticles for *in vivo* targeted drug delivery. *Biomaterials*. 2007;**28**(5):869-876. DOI: 10.1016/j.biomaterials.2006.09.047

[83] Manson J, Kumar D, Meenan BJ, Dixon D. Polyethylene glycol functionalized gold nanoparticles: The influence of capping density on stability in various media. *Gold Bulletin*. 2011;**44**(2):99-105. DOI: 10.1007/s13404-011-0015-8

[84] Maldiney T, Richard C, Seguin J, Wattier N, Bessodes M, Scherman D. Effect of core diameter, surface coating, and PEG chain length on the biodistribution of persistent luminescence nanoparticles in mice. *ACS Nano*. 2011;**5**(2):854-862. DOI: 10.1021/nn101937h

[85] Buchman YK, Lellouche E, Zigdon S, Bechor M, Michaeli S, Lellouche JP. Silica nanoparticles and polyethyleneimine (PEI)-mediated functionalization: A new method of PEI covalent attachment for siRNA delivery applications. *Bioconjugate Chemistry*. 2013;**24**(12):2076-2087. DOI: 10.1021/bc4004316

[86] Liu C, Wang Z, Wang X, Li Z. Surface modification of hydrophobic NaYF<sub>4</sub>: Yb, Er upconversion nanophosphors and their applications for immunoassay. *Science China. Chemistry*. 2011;**54**(8):1292-1297. DOI: 10.1007/s11426-011-4319-6

[87] Rao J, Dragulescu-Andrasi A, Yao H. Fluorescence imaging *in vivo*: Recent advances. *Current Opinion in Biotechnology* [Internet]. 2007;**18**(1):17-25. DOI: 10.1016/j.copbio.2007.01.003

[88] Yang D, Dai Y, Ma P, Kang X, Cheng Z, Li C, et al. One-step synthesis of small-sized and water-soluble NaREF<sub>4</sub> upconversion nanoparticles for *In vitro* cell

- imaging and drug delivery. *Chemistry – A European Journal*. 2013;**19**(8):2685-2694. DOI: 10.1002/chem.201203634
- [89] Suvorov NV, Mironov AF, Grin MA. Folic acid and its derivatives for targeted photodynamic therapy of cancer. *Russian Chemical Bulletin*. 2017;**66**:1982-2008. DOI: 10.1007/s11172-017-1973-7
- [90] Xie A, Tsvetkova I, Liu Y, Ye X, Hewavitharanage P, Dragnea B, et al. Hydrophobic cargo encapsulation into virus protein cages by self-assembly in an aprotic organic solvent. *Bioconjugate Chemistry*. 2021;**32**(11):2366-2376. DOI: 10.1021/acs.bioconjchem.1c00420
- [91] Klymchenko A, Duportail G, Mely Y. *Fluorescent methods to study biological membranes*. Springer Series on Fluorescence. 2013;**13**:51-70. DOI: 10.1007/4243\_2012\_44
- [92] Hong G, Antaris AL, Dai H. Near-infrared fluorophores for biomedical imaging. *Nature Biomedical Engineering [Internet]*. 2017;**1**(1):10. DOI: 10.1038/s41551-016-0010
- [93] Hsu HJ, Bugno J, Sr L, Hong S. Dendrimer-based nanocarriers: A versatile platform for drug delivery. *Wiley Interdisciplinary Reviews - Nanomedicine and Nanobiotechnology*. 2017;**9**:e1409. DOI: 10.1002/wnan.1409
- [94] Dong H, Du SR, Zheng XY, Lyu GM, Sun LD, Li LD, et al. Lanthanide nanoparticles: From design toward bioimaging and therapy. *Chemical Reviews*. American Chemical Society. 2015;**115**:10725-10815. DOI: 10.1021/acs.chemrev.5b00091
- [95] Yu M, Li F, Chen Z, Hu H, Zhan C, Yang H, et al. Laser scanning up-conversion luminescence microscopy for imaging cells labeled with rare-earth nanophosphors. *Analytical Chemistry*. 2009;**81**(3):930-935. DOI: 10.1021/ac802072d
- [96] Jin J, Gu YJ, Man CWY, Cheng J, Xu Z, Zhang Y, et al. Polymer-coated NaYF<sub>4</sub>: Yb<sup>3+</sup>, Er<sup>3+</sup> upconversion nanoparticles for charge-dependent cellular imaging. *ACS Nano*. 2011;**5**(10):7838-7847. DOI: 10.1021/nn201896m
- [97] Tsang MK, Chan CF, Wong KL, Hao J. Comparative studies of upconversion luminescence characteristics and cell bioimaging based on one-step synthesized upconversion nanoparticles capped with different functional groups. *Journal of Luminescence*. 2015;**157**:172-178. DOI: 10.1016/j.jlumin.2014.08.057
- [98] Chávez-García D, Juárez-Moreno K, Reyes R, Barrera J, Hirata GA. Nanotoxicological assessments to warranty the use of functionalized Y<sub>2</sub>O<sub>3</sub> nanoparticles for biomedical applications. *Advanced Materials Letters*. 2020;**11**(12):1-9. DOI: 10.5185/amlett.2020.121583
- [99] Del Rosal B, Jaque D. Upconversion nanoparticles for *in vivo* applications: Limitations and future perspectives. *Methods and Applications in Fluorescence*. 2019;**7**(2):022001. DOI: 10.1088/2050-6120/ab029f
- [100] Ortgies DH, Tan M, Ximendes EC, del Rosal B, Hu J, Xu L, et al. Lifetime-encoded infrared-emitting nanoparticles for *in vivo* multiplexed imaging. *ACS Nano*. 2018;**12**(5):4362-4368. DOI: 10.1021/acsnano.7b09189
- [101] Zhan Q, Qian J, Liang H, Somesfalean G, Wang D, He S, et al. Using 915 nm laser excited Tm<sup>3+</sup>/Er<sup>3+</sup>/Ho<sup>3+</sup>-doped NaYbF<sub>4</sub> upconversion nanoparticles for *in vitro* and deeper *in vivo* bioimaging without overheating irradiation. *ACS Nano*.



2011;5(5):3744-3757. DOI: 10.1021/nn200110j

[102] Xiong LQ, Chen ZG, Yu MX, Li FY, Liu C, Huang CH. Synthesis, characterization, and *in vivo* targeted imaging of amine-functionalized rare-earth up-converting nanophosphors. *Biomaterials*. 2009;30(29):5592-5600. DOI: 10.1016/j.biomaterials.2009.06.015

[103] Zeng S, Tsang MK, Chan CF, Wong KL, Hao J. PEG modified BaGdF5:Yb/Er nanoprobes for multimodal upconversion fluorescent, *in vivo* X-ray computed tomography and biomagnetic imaging. *Biomaterials*. 2012;33(36):9232-9238. DOI: 10.1016/j.biomaterials.2012.09.019

[104] Hilderbrand SA, Shao F, Salthouse C, Mahmood U, Weissleder R. Upconverting luminescent nanomaterials: Application to *in vivo* bioimaging. *Chemical Communications*. 2009;28:4188-4190. DOI: 10.1039/B905927J

[105] Han S, Deng R, Xie X, Liu X. Enhancing luminescence in lanthanide-doped upconversion nanoparticles. *Angewandte Chemie - International Edition*. 2014;53:11702-11715

[106] Mosmann T. Rapid colorimetric assay for cellular growth and survival: Application to proliferation and cytotoxicity assays. *Journal of Immunological Methods*. 1983;65(1-2):55-63. DOI: 10.1016/0022-1759(83)90303-4

[107] Shan J, Chen J, Meng J, Collins J, Soboyejo W, Friedberg JS, et al. Biofunctionalization, cytotoxicity, and cell uptake of lanthanide doped hydrophobically ligated NaYF<sub>4</sub> upconversion nanophosphors. *Journal of Applied Physics*. 2008;104(9):094308. DOI: 10.1063/1.3008028

[108] Di Meo S, Reed TT, Venditti P, Victor VM. Role of ROS and RNS Sources

in Physiological and Pathological Conditions. In: *Oxidative Medicine and Cellular Longevity*. London UK: Hindawi Publishing Corporation; 2016. DOI: 10.1155/2016/1245049

[109] Regoli F, Giuliani ME. Oxidative pathways of chemical toxicity and oxidative stress biomarkers in marine organisms. *Marine Environmental Research*. 2014;93:106-117. DOI: 10.1016/j.marenvres.2013.07.006

[110] Shapiro HM. *Practical Flow Cytometry*. Hoboken, New Jersey: John Wiley & Sons, Inc; 2003. p. 724

[111] Van Engeland M, Nieland LJW, Ramaekers FCS, Schutte B, Reutelingsperger CPM. Annexin V-affinity assay: A review on an apoptosis detection system based on phosphatidylserine exposure. *Cytometry*. 1998;31(1):1-9. DOI: 10.1002/(SICI)1097-0320(19980101)31:1<1::AID-CYTO1>3.0.CO

[112] Riedl SJ, Shi Y. Molecular mechanisms of caspase regulation during apoptosis. *Nature Reviews. Molecular Cell Biology*. 2004;5(11):897-907. DOI: 10.1038/nrm1496

[113] Vermes I, Haanen C, Steffens-Nakken H, Reutelingsperger C. A novel assay for apoptosis flow cytometric detection of phosphatidylserine expression on early apoptotic cells using fluorescein labelled Annexin V. *Journal of Immunological Methods*. 1995;184(1):39-51. DOI: 10.1016/0022-1759(95)00072-I

[114] Das GK, Sudheendra L, Kennedy IM. Heterogeneous nanostructures for plasmonic interaction with luminescence and quantitative surface-enhanced Raman spectroscopy. *Reporters, Markers, Dyes, Nanoparticles, and Molecular Probes for Biomedical Applications VI*. 2014;8956:89560X. DOI: 10.1117/12.2037889

- [115] Stone N, Kendall C, Smith J, Crow P, Barr H. Raman spectroscopy for identification of epithelial cancers. *Faraday Discussions*. 2004;**126**:141-157. DOI: 10.1039/B304992B
- [116] Brauchle E, Thude S, Brucker SY, Schenke-Layland K. Cell death stages in single apoptotic and necrotic cells monitored by Raman microspectroscopy. *Scientific Reports*. 2014;**4**:4698. DOI: 10.1038/srep04698
- [117] Karlsson HL, Di Bucchianico S, Collins AR, Dusinska M. Can the comet assay be used reliably to detect nanoparticle-induced genotoxicity? *Environmental and Molecular Mutagenesis*. 2015;**56**(2):82-96. DOI: 10.1002/em.21933
- [118] Azqueta A, Gutzkow KB, Priestley CC, Meier S, Walker JS, Brunborg G, et al. A comparative performance test of standard, medium- and high-throughput comet assays. *Toxicology in Vitro*. 2013;**27**(2):768-773. DOI: 10.1016/j.tiv.2012.12.006
- [119] Speit G, Hartmann A. The comet assay. In: Henderson DS, editor. *DNA Repair Protocols: Mammalian Systems*. Totowa, NJ: Humana Press; 2006. pp. 275-286. DOI: 10.1385/1-59259-973-7:275
- [120] Hamblin MR. Upconversion in photodynamic therapy: Plumbing the depths. *Dalton Transactions*. 2018;**47**(26):8571-8580. DOI: 10.1039/C8DT00087E
- [121] Nigoghossian K, Saska S, Christovam LM, Coelho F, Beatrice CAG, Lucas AA, et al. Upconversion 3D printed composite with multifunctional applications for tissue engineering and photodynamic therapy. *Journal of the Brazilian Chemical Society*. 2020;**31**(4):638-652. DOI: 10.21577/0103-5053.20190228
- [122] Doronkina A, Kazadaeva N, Sagaidachnaya E, Yanina I, Skaptsov A, Konyukhova Y, et al. Erythrocyte aggregation stimulated by NaYF<sub>4</sub>: Er<sup>3+</sup>, Yb<sup>3+</sup> upconversion nanoparticles. *Proceedings Saratov Fall Meeting 2019: Optical and Nano-Technologies for Biology and Medicine*. 2020;**114570**:11457D. DOI: 10.1117/12.2559853
- [123] Chatterjee DK, Rufaihah AJ, Zhang Y. Upconversion fluorescence imaging of cells and small animals using lanthanide doped nanocrystals. *Biomaterials*. 2008;**29**(7):937-943. DOI: 10.1016/j.biomaterials.2007.10.051
- [124] Wang M, Mi CC, Wang WX, Liu CH, Wu YF, Xu ZR, et al. Immunolabeling and NIR-excited fluorescent imaging of HeLa cells by using NaYF<sub>4</sub>: Yb, Er upconversion nanoparticles. *ACS Nano*. 2009;**3**(6):1580-1586. DOI: 10.1021/nn900491j
- [125] Abdul Jalil R, Zhang Y. Biocompatibility of silica coated NaYF<sub>4</sub> upconversion fluorescent nanocrystals. *Biomaterials*. 2008;**29**(30):4122-4128. DOI: 10.1016/j.biomaterials.2008.07.012
- [126] Punjabi A, Wu X, Tokatli-Apollon A, El-Rifai M, Lee H, Zhang Y, et al. Amplifying the red-emission of upconverting nanoparticles for biocompatible clinically used prodrug-induced photodynamic therapy. *ACS Nano*. 2014;**8**(10):10621-10630. DOI: 10.1021/nn505051d
- [127] Jiang S, Zhang Y, Lim KM, Sim EKW, Ye L. NIR-to-visible upconversion nanoparticles for fluorescent labeling and targeted delivery of siRNA. *Nanotechnology*. 2009;**20**(15):155101. DOI: 10.1088/0957-4484/20/15/155101
- [128] Vetrone F, Naccache R, Juarranz De La Fuente A, Sanz-Rodríguez F, Blazquez-Castro A, Rodríguez EM, et al.

Intracellular imaging of HeLa cells by non-functionalized NaYF<sub>4</sub>: Er<sup>3+</sup>, Yb<sup>3+</sup> upconverting nanoparticles. *Nanoscale*. 2010;2(4):495-498. DOI: 10.1039/B9NR00236G

[129] Hu H, Yu M, Li F, Chen Z, Gao X, Xiong L, et al. Facile epoxidation strategy for producing amphiphilic up-converting rare-earth nanophosphors as biological labels. *Chemistry of Materials*. 2008;20(22):7003-7009. DOI: 10.1021/cm801215t

[130] Juarez-Moreno K, Chávez-García D, Hirata G, Vazquez-Duhalt R. Monolayer (2D) or spheroids (3D) cell cultures for nanotoxicological studies. Comparison of cytotoxicity and cell internalization of nanoparticles. *Toxicology in Vitro*. 2022;85:105461. DOI: 10.1016/j.tiv.2022.105461

[131] Liu Y, Hou W, Sun H, Cui C, Zhang L, Jiang Y, et al. Thiol-ene click chemistry: A biocompatible way for orthogonal bioconjugation of colloidal nanoparticles. *Chemical Science*. 2017;8(9):6182-6187. DOI: 10.1021/cm801215t

[132] Chen Y, D'Amario C, Gee A, Duong HTT, Shimoni O, Valenzuela SM. Dispersion stability and biocompatibility of four ligand-exchanged NaYF<sub>4</sub>: Yb, Er upconversion nanoparticles. *Acta Biomater*. 2020;102:384-393. DOI: 10.1016/j.actbio.2019.11.048

[133] M. Ekkapongpisit, A. Giovia, C. Follo, G. Caputo & . Isidoro, C. Biocompatibility, endocytosis, and intracellular trafficking of mesoporous silica and polystyrene nanoparticles in ovarian cancer cells: Effects of size and surface charge groups. *International Journal of Nanomedicine* 2012; 2012. 4147-4158. DOI: 10.2147/IJN.S33803

[134] Ichimura T, Jin T, Fujita H, Higuchi H, Watanabe TM. Nano-scale

measurement of biomolecules by optical microscopy and semiconductor nanoparticles. *Frontiers in Physiology*. 2014;5:273. DOI: 10.3389/fphys.2014.00273

[135] Tsai S, Chen Y, Liaw JW. Compound cellular imaging of laser scanning confocal microscopy by using gold nanoparticles and dyes. *Sensors*. 2008;8(4):2306-2316. DOI: 10.3390/s8042306